AD-A072 750 OHIO STATE UNIV COLUMBUS ELECTROSCIENCE LAB F/G 9/3
A LOOP FOR TRACKING THE FREQUENCY OF A PULSED SINUSOID.(U)
JUL 79 R J HUFF, D W HERR F30602-75-C-0061
UNCLASSIFIED ESL-710300-4 RADC-TR-79-171 NL

| OF |
AD
A072750

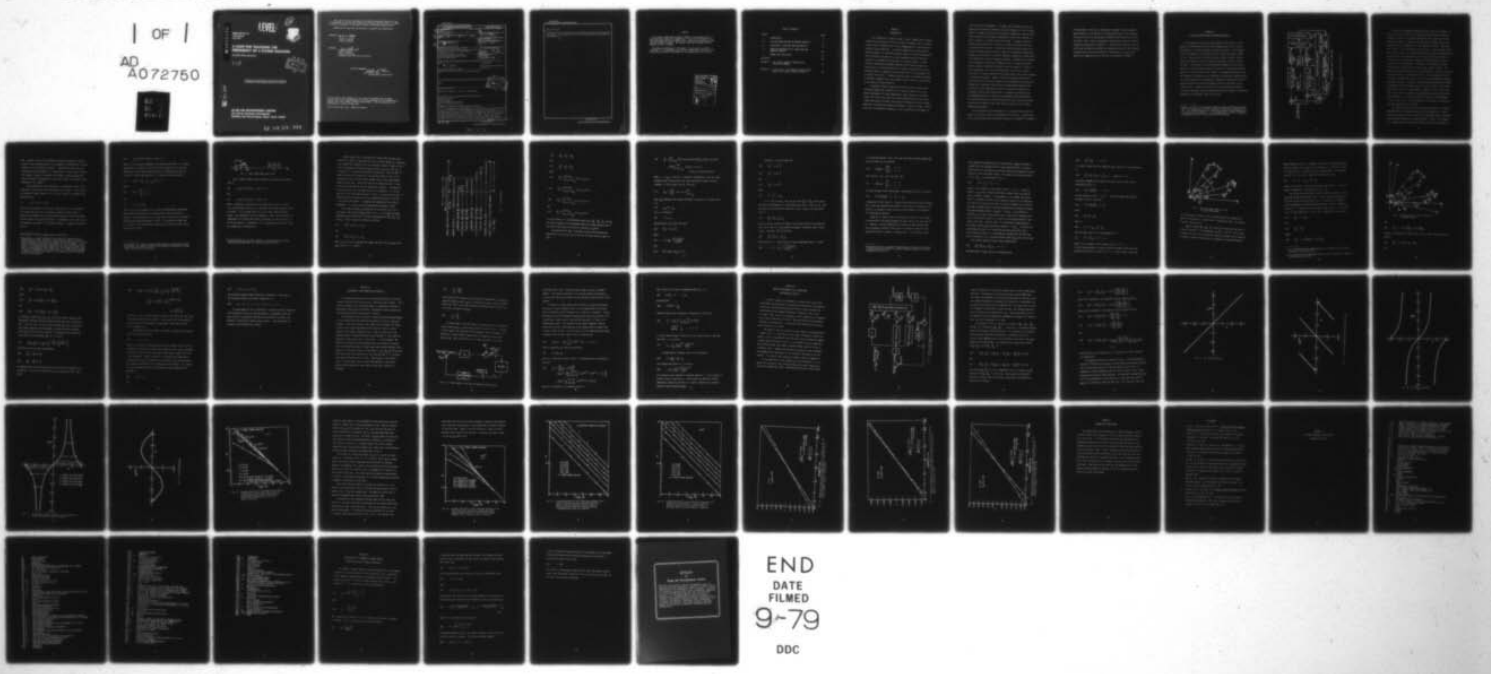

END
DATE
FILMED
9-79
DDC

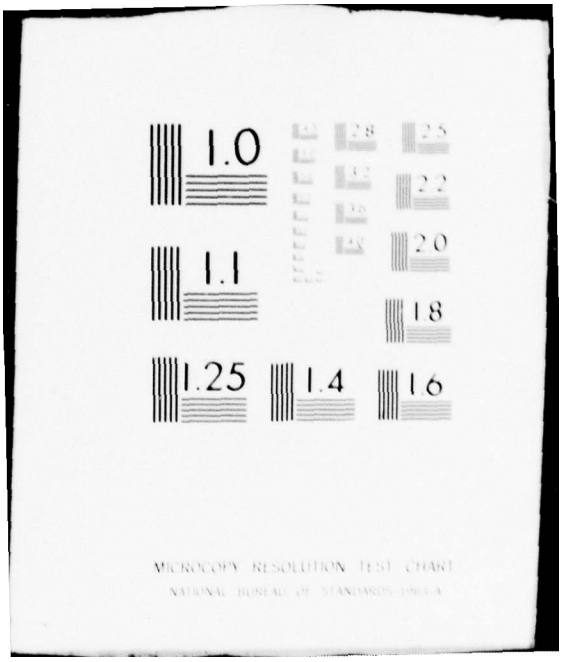
1.0
1.1
1.25
1.4
1.6
2.0
2.2
2.5
MICROCOPY RESOLUTION TEST CHART
NATIONAL BUREAU OF STANDARDS 1963-A

LEVEL II

RADC-TR-79-171
Interim Report
July 1979

A LOOP FOR TRACKING THE FREQUENCY OF A PULSED SINUSOID

The Ohio State University

R. J. Huff
D. W. Herr

ROME AIR DEVELOPMENT CENTER
Air Force Systems Command
Griffiss Air Force Base, New York 13441

This report has been reviewed by the RADC Information Office (OI) and is releasable to the National Technical Information Service (NTIS). At NTIS it will be releasable to the general public, including foreign nations.

RADC-TR-79-171 has been reviewed and is approved for publication.

APPROVED: Stuart H. Talbot

STUART H. TALBOT
Project Engineer

APPROVED: Fred I. Diamond

FRED I. DIAMOND
Technical Director
Communications and Control Division

FOR THE COMMANDER: John P. Huss

JOHN P. HUSS
Acting Chief, Plans Office

If your address has changed or if you wish to be removed from the RADC mailing list, or if the addressee is no longer employed by your organization, please notify RADC (DCCR), Griffiss AFB NY 13441. This will assist us in maintaining a current mailing list.

Do not return this copy. Retain or destroy.

UNCLASSIFIED

SECURITY CLASSIFICATION OF THIS PAGE (When Data Entered)

REPORT DOCUMENTATION PAGE

READ INSTRUCTIONS BEFORE COMPLETING FORM

1. REPORT NUMBER: RADC-TR-79-171	2. GOVT ACCESSION NO.
3. RECIPIENT'S CATALOG NUMBER	
4. TITLE (and Subtitle): A LOOP FOR TRACKING THE FREQUENCY OF A PULSED SINUSOID	5. TYPE OF REPORT & PERIOD COVERED: Interim Report
6. PERFORMING ORG. REPORT NUMBER: ESL-710300-4	
7. AUTHOR(s): R. J. Huff, D. W. Herr	8. CONTRACT OR GRANT NUMBER(s): F30602-75-C-0061
9. PERFORMING ORGANIZATION NAME AND ADDRESS: The Ohio State University/ElectroScience Laboratory, Department of Electrical Engineering, Columbus OH 43121	10. PROGRAM ELEMENT, PROJECT, TASK AREA & WORK UNIT NUMBERS: 62702F, 65230907, 09
11. CONTROLLING OFFICE NAME AND ADDRESS: Rome Air Development Center (DCCR), Griffiss AFB NY 13441	12. REPORT DATE: July 1979
	13. NUMBER OF PAGES: 61
14. MONITORING AGENCY NAME & ADDRESS (if different from Controlling Office): Same	15. SECURITY CLASS. (of this report): UNCLASSIFIED
	15a. DECLASSIFICATION/DOWNGRADING SCHEDULE: N/A

16. DISTRIBUTION STATEMENT (of this Report)

Approved for public release, distribution unlimited.

17. DISTRIBUTION STATEMENT (of the abstract entered in Block 20, if different from Report)

Same

18. SUPPLEMENTARY NOTES

RADC Project Engineer: Stuart H. Talbot (DCCR)

19. KEY WORDS (Continue on reverse side if necessary and identify by block number)

Frequency trading
Pulse signals
Digital communication systems
Time Division Multiple Access

20. ABSTRACT (Continue on reverse side if necessary and identify by block number)

The configuration and performance of a hybrid frequency tracking loop which tracks the frequency of a pulsed sinusoid are addressed in this report. A linear model of the loop is developed and an approximate expression is derived for the standard deviation of the frequency tracking error due to the presence of additive white Gaussian noise at the loop's input. Results obtained by simulating the loop on a digital computer are presented which show the extent to which loop non-linearities affect the standard deviation of the frequency → next page (Cont'd)

DD FORM 1 JAN 73 1473

UNCLASSIFIED

SECURITY CLASSIFICATION OF THIS PAGE (When Data Entered)

402 251

Item 20 (Cont'd)

tracking error, the distribution of the frequency tacking error, and the loop lock range. These results show that the loop operates with a high degree of effectiveness.

PREFACE

This report, OSURF Report Number 710300-4, was prepared by the ElectroScience Laboratory, Department of Electrical Engineering, The Ohio State University at Columbus, Ohio. Research was conducted under Contract F30602-75-C-0061. Mr. Stuart Talbot was the RADC Program Monitor for this research.

The material contained in this report is also used as a Thesis submitted to the Department of Electrical Engineering, The Ohio State University as partial fulfillment for the degree Master of Science.

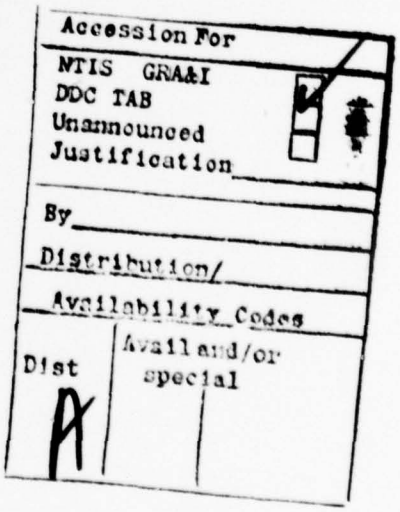

TABLE OF CONTENTS

CHAPTER I

INTRODUCTION

The frequencies of signals present in radio communication systems often differ from design values as a result of doppler and/or oscillator instabilities by amounts which, if not compensated for, would preclude effective signal detection. In digital communication systems wherein received signals are coherently detected, phase lock loops are generally used to maintain the phases of signals generated locally within the receivers in alignment with the phases of received signals. Differentially coherent and incoherent detectors do not require phase synchronization for proper operation, but frequency uncertainties must be maintained small in comparison with the data rate if such detectors are to operate efficiently. Frequency tracking loops are generally employed to maintain frequency errors at acceptably small values in systems which do not contain coherent detectors.

A frequency tracking loop would ideally operate to maintain the difference between the frequencies of a received signal (or an intermediate-frequency (IF) signal generated by down-converting a received signal) and a local oscillator (LO) signal generated within the loop at a specified value by suitably controlling the frequency of the LO signal. Generally, the specified frequency difference is equal to either a design value for an intermediate frequency or zero, depending on the manner in

which the loop is implemented. In either case, suitable circuits are employed to estimate the amount by which the frequency of the LO signal should be changed to maintain the difference frequency at the specified value, and the error estimate is employed to control the frequency of the LO signal in a suitable closed-loop manner. Frequency control is generally made possible by utilizing a voltage controlled oscillator to generate the LO signal. In loops which would ideally maintain frequency differences equal to design values for intermediate frequencies, frequency discriminators are usually employed to generate voltages which are proportional to the LO frequency errors[1]. Coherent cycle counting can be employed to estimate LO frequency errors in loops which would ideally maintain frequency differences equal to zero[2,3]. Either of these approaches can be utilized effectively in practical systems -- particularly in systems wherein the received signals have either constant or continuous envelopes. However, should the received signal have a pulsed envelope, the minimum frequency error detectable using practical coherent cycle counting circuits would be approximately equal to the reciprocal of the signal-pulse duration: a value which would be unacceptably large in many applications. Frequency discrimination can be implemented which will operate with reasonable effectiveness when the received signal has a pulsed envelope, but such circuits are analog devices and are generally less than ideally suited for use in modern communication systems.

The configuration and performance of a loop which tracks the frequency of a pulsed sinusoid are addressed in this thesis. A description of the loop and applicable preliminary analyses are presented in Chapter II.

A linear model of the loop is developed in Chapter III and an approximate expression is derived for the standard deviation of the frequency tracking error due to the presence of additive white Gaussian noise at the loop's input. Results obtained by simulating the loop on a digital computer are presented in Chapter IV. These results show the extent to which loop nonlinearities affect the standard deviation of the frequency tracking error and the distribution of the frequency tracking error. Results are summarized and conclusions are presented in Chapter V.

CHAPTER II

LOOP CONFIGURATION AND PRELIMINARY ANALYSES

The frequency tracking loop investigated in this thesis is presumed to be representable by the block diagram given in Fig. 1 and is designated as the hybrid frequency tracking loop (HFTL). This designation is considered to be appropriate since a loop configured as shown in Fig. 1 would consist of analog circuits, digital circuits, and circuits which would be partially analog and partially digital in nature. The HFTL is structured so that the difference between the carrier frequency of a desired signal present at the input to the loop and the frequency of a local oscillator (LO) signal is estimated periodically, and the frequency difference (error) estimates are processed to generate digital control words which are applied in sequence to the control input of a digitally-controlled variable-frequency oscillator (D-C/VFO): the LO-signal source.* Ideally, the digital control word would be varied so that the LO frequency would be maintained identically equal to the carrier frequency of the desired signal at all times.

---

*Either a D-C/VFO or a conventional analog voltage-controlled oscillator (VCO) can be employed in a HFTL to generate a variable-frequency LO signal. The preferred approach to effecting frequency control depends on the application of interest. It is presumed that a D-C/VFO is employed to implement the HFTL for explicitness of discussion.

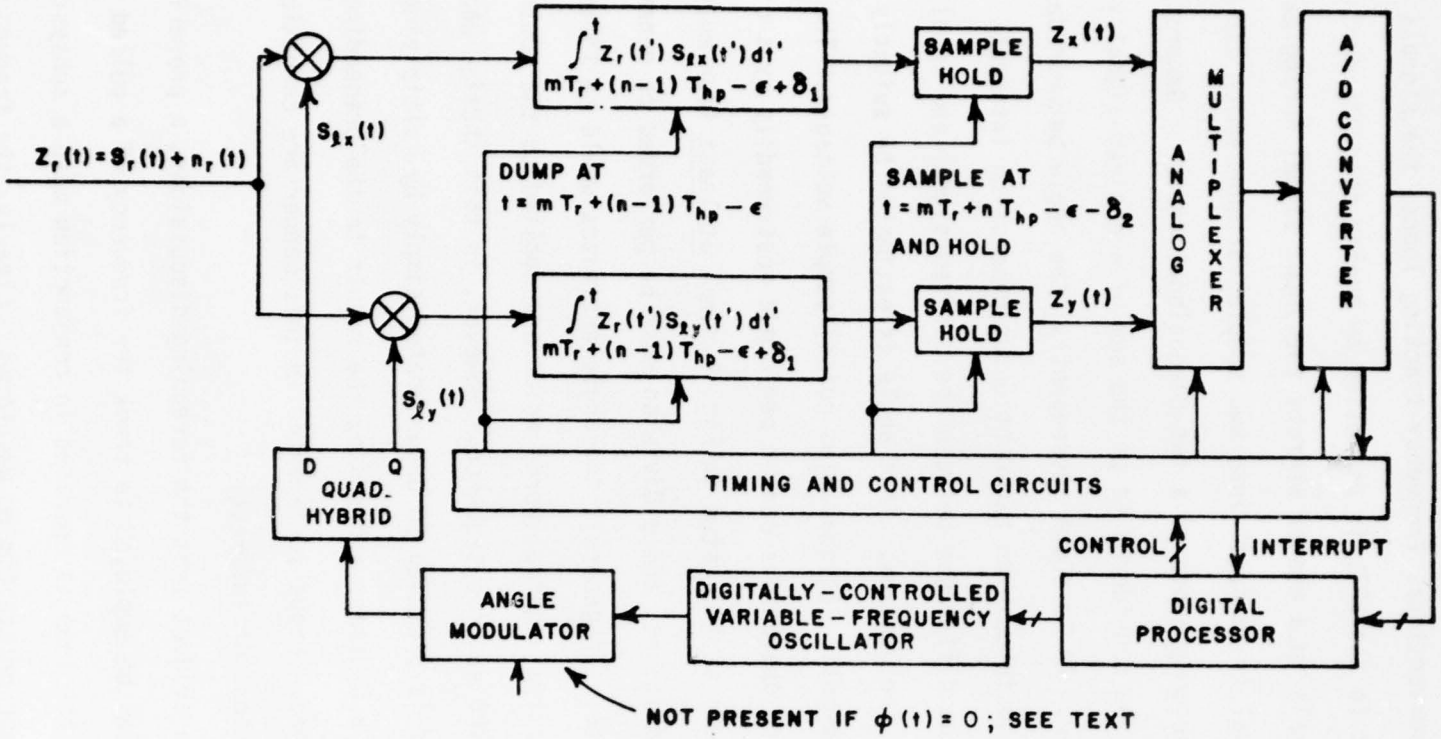

Fig. 1. Block diagram of the hybrid (analog and digital) frequency tracking loop.

Unlike in conventional frequency-tracking loops, the signals present at the input to the HFTL is processed by analog circuits during successive intervals in a manner whereby the input signal during each processing interval is "mapped" into two sample voltages which can be interpreted as the components of a two-dimensional vector. Generally, each "vector" can be considered to be the sum of a desired-signal vector and a noise vector. As is shown subsequently, the angle between desired-signal vectors associated with two contiguous processing intervals is proportional to the difference between the desired signal and local oscillator signal frequencies. That angle is estimated by suitably processing four composite (signal plus noise) sample voltages. The required processing operations can be performed most readily by a digital processor (computer) as indicated in Fig. 1 since at least four multiplications, two additions, and a division must be performed to generate each angle estimate. In general, the angle estimates would be filtered to generate the ditigal control words which are applied to the control input of the D-C/VFO in time sequence. However, in this thesis, each "new" control word is presumed to be generated simply by multiplying an angle estimate by a constant and adding the result to the preceeding ("old") control word. Loops implemented in this manner are compatible with many applications of interest.

As should be evident from the foregoing discussions, a properly-implemented HFTL can be employed to track the frequency of a pulsed sinusoid provided the loop is operated in conjunction with a subsystem which generates appropriate timing waveforms. Clearly, the frequency of a sinusoid having a continuous envelope could also be tracked by a

HFTL. However, HFTLs are envisioned as being used primarily in applications of the preceding type; it is subsequently presumed that a pulsed sinusoid is to be tracked by the HFTL. A mathematical basis for proceeding with the development of a linear model of a HFTL and for employing a digital computer to simulate a HFTL when a pulsed sinusoid and noise are present simultaneously at the loop's input is presented in the remainder of this chapter.

The performance of a HFTL depends to a considerable extent on the properties of the signal and noise present at its input. In this thesis, the composite signal present in the input to the HFTL is presumed to be expressible as*

$$(1) \qquad Z_r(t) \triangleq S_r(t) + n_r(t)$$

where $S_r(t)$ represents the "desired" signal and $n_r(t)$ is considered to be a sample function from a stationary stochastic process which is Gaussian distributed with zero mean and white with a single-sided power spectral density of N_o watts per Hertz. Furthermore, noise process $n_r(t)$ is assumed to be ergodic.** The desired signal is assumed to be expressible as

---

* The symbol $\triangleq$ is used to denote equal by definition.

**Occasionally, a single notation is used herein to represent both a sample function from a stochastic process and the family of functions which constitute that process; the appropriate interpretation of a given notation should be clear from the context in which it appears. Hereafter, it is presumed without elaboration that selected ensemble averages to be calculated are each equal to a time average which describes, in part, the performance of a single HFTL, i.e., that selected random responses of the HFTL are ergodic in an appropriate sense in addition to $n_r(t)$ being ergodic.

(2) $$s_r(t) \triangleq A_r(t) \sin[\omega_r t + \phi(t) + \alpha]$$

where ω_r is the radian frequency to be tracked by the HFTL, α is a phase angle which is constant at any value in the interval $[-\pi,\pi]$, and $\phi(t)$ represents a (any) phase modulation which is reproducible within the receiver.* Signal amplitude $A_r(t)$ is assumed to be expressible as

(3) $$A_r(t) \triangleq \sqrt{2P_r} \sum_{m=-\infty}^{\infty} P_{T_{hp}}(t - m T_r)$$

where

(4) $$P_T(t) \triangleq \begin{cases} 1 & |t| < T \\ 0 & |t| > T \end{cases}$$

and

(5) $$T_r > T_p \triangleq 2T_{hp} \quad .$$

That is, $A_r(t)$ is presumed to be a train of nonoverlapping rectangular pulses which are generated at a uniform rate of one pulse every T_r seconds. As illustrated in Fig. 2, each pulse in $A_r(t)$ has a T_p second duration and an amplitude equal to $\sqrt{2P_r}$. It can easily be shown that P_r is equal to the average power contained in the desired signal during the pulse "on" times.

---

*For example, in a digital biphase spread-spectrum communication system application, $\phi(t)$ would be equal to $C(t)\pi$ where $C(t)$ represents a known binary pseudo-noise (PN) sequence.

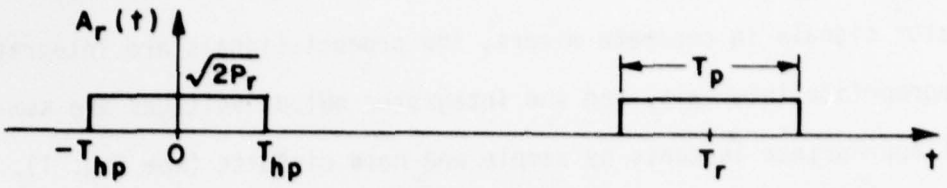

Fig. 2. Signal amplitude versus time.

The LO signals present within the HFTL are assumed to be expressible as

$$(6) \qquad s_{\ell x}(t) \triangleq A_\ell \sin[\omega_\ell t + \phi(t+\varepsilon) + \beta]$$

and

$$(7) \qquad s_{\ell y}(t) \triangleq A_\ell \cos[\omega_\ell t + \phi(t+\varepsilon) + \beta]$$

where ε represents a timing error associated with a receive clock,* β is a constant phase angle, and ω_ℓ represents the radian frequency of the LO signals. It is assumed that all circuits have unlimited dynamic ranges. One consequence of this assumption is that loop performance is independent of LO-signal amplitude A_ℓ (provided, of course, that A_ℓ is finite and nonzero). Subsequently, it is presumed that A_ℓ equals $\sqrt{2/T_{hp}}$ for convenience of presentation.

*As noted previously, the HFTL operates in conjunction with a timing subsystem which generates all required timing waveforms.

Input signal $Z_r(t)$ is multiplied by (mixed with) the two local oscillator signals in separate mixers, the product signals are integrated over appropriate intervals, and the integrator output voltages are sampled at appropriate instants by sample and hold circuits (see Fig. 1). If the HFTL is to operate efficiently, timing error ε must be small in comparison with the reciprocal of the spectral width of $\phi(t)$ if the spectrum of $S_r(t)$ is sufficiently "spread" due to $\phi(t)$ being nonzero. Should $\phi(t)$ be zero, ε would only need to be maintained small in comparison with the duration of the integration intervals. Irrespective of the nature of $\phi(t)$, the dump time of the integrators, δ_1, and the aperture time of the sample and hold circuits, δ_2, must each be small in comparison with the duration of the integration intervals if the HFTL is to operate efficiently. Throughout the remainder of this thesis, parameters ε, δ_1, and δ_2 are each considered to be equal to zero.

Four sample voltages are generated for each pulse in $s_r(t)$ as indicated on the timing diagram shown in Fig. 3. The sample voltages generated by processing the m^{th} pulse are designated as Z_{0x}^m, Z_{0y}^m, Z_{1x}^m, and Z_{1y}^m. These voltages are defined as follows:

$$Z_{nx}^m \triangleq Z_x(m\,T_r + n\,T_{hp}) \tag{8}$$

and

$$Z_{ny}^m \triangleq Z_y(m\,T_r + n\,T_{hp}) \tag{9}$$

where $Z_x(t)$ and $Z_y(t)$ represent the sample and hold circuit output voltages (see Fig. 1). Clearly,

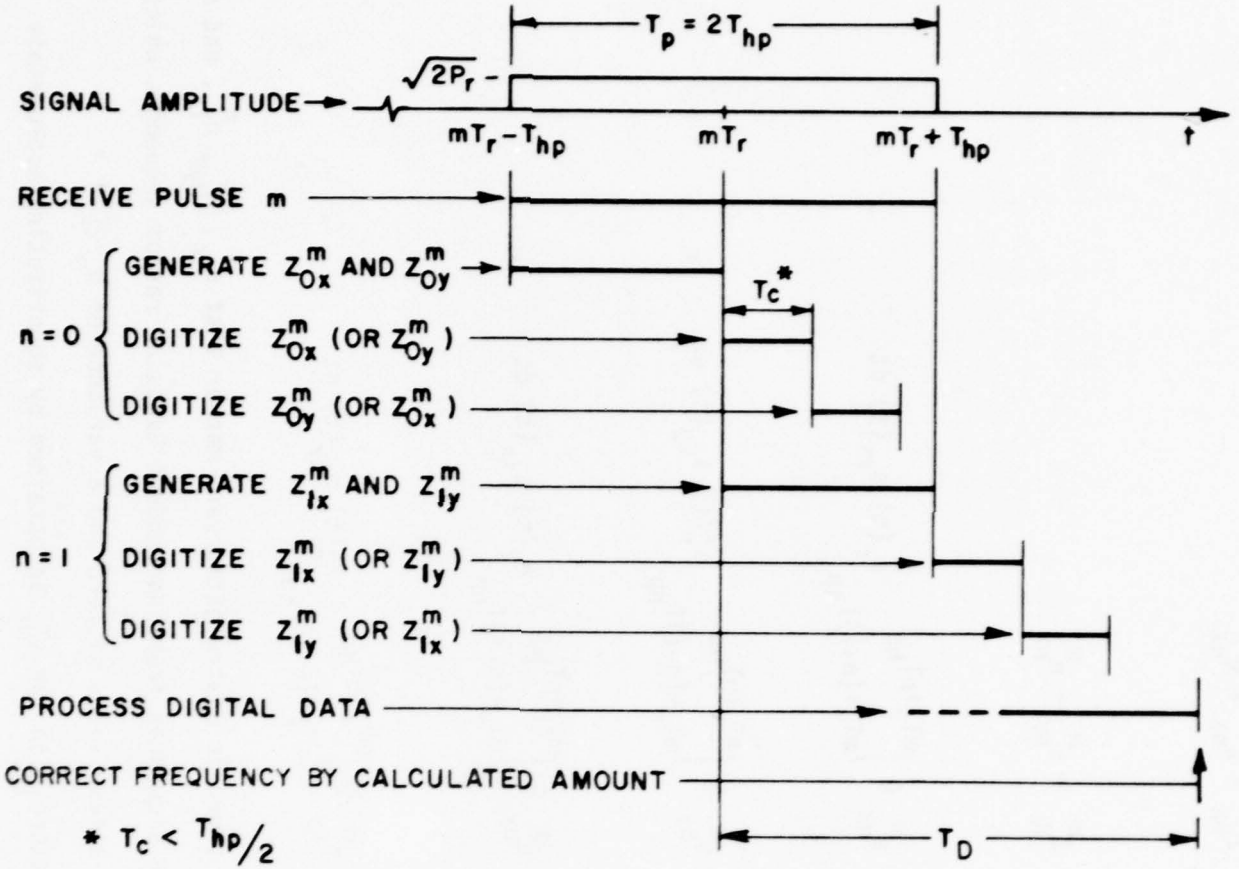

Fig. 3. Timing diagram.

$$Z_{nx}^{m} = s_{nx}^{m} + n_{nx}^{m} \tag{10}$$

and

$$Z_{ny}^{m} = s_{ny}^{m} + n_{nx}^{m} \tag{11}$$

where

$$s_{nx}^{m} \triangleq \int_{mT_r+(n-1)T_{hp}}^{mT_r+nT_{hp}} s_r(t)\, s_{\ell x}(t)\, dt \quad , \tag{12}$$

$$s_{ny}^{m} \triangleq \int_{mT_r+(n-1)T_{hp}}^{mT_r+nT_{hp}} s_r(t)\, s_{\ell y}(t)\, dt \quad , \tag{13}$$

$$n_{nx}^{m} \triangleq \int_{mT_r+(n-1)T_{hp}}^{mT_r+nT_{hp}} n_r(t)\, s_{\ell x}(t)\, dt \quad , \tag{14}$$

and

$$n_{ny}^{m} \triangleq \int_{mT_r+(n-1)T_{hp}}^{mT_r+nT_{hp}} n_r(t)\, s_{\ell y}(t)\, dt \quad . \tag{15}$$

It can be shown in a straightforward manner that n_{0x}^{m}, n_{0y}^{m}, n_{1x}^{m}, and n_{1y}^{m} are sample sequences from independent Gaussian random sequences which each have a mean value of zero and a variance of $N_o/2$[4].

An expression for s_{0x}^{m} is obtained by substituting appropriate expressions for $s_r(t)$ and $s_{\ell x}(t)$ into Eq. (12) and setting n equal to zero:

$$(16)\qquad s_{0x}^{m} = \int_{mT_r-T_{hp}}^{mT_r} \sqrt{2P_r}\,\sin[\omega_r t+\phi(t)+\alpha]\sqrt{2/T_{hp}}\,\sin[\omega_\ell t+\phi(t)+\beta]dt$$

$$= \sqrt{P_r/T_{hp}} \int_{mT_r-T_{hp}}^{mT_r} \{\cos[(\omega_r-\omega_\ell)t+\alpha-\beta] - \cos[(\omega_r+\omega_\ell)t+2\phi(t)+\alpha+\beta]\}dt\ .$$

When $\omega_r >> \pi/T_{hp}$ or the HFTL is otherwise implemented so that the upper sideband signals generated by the mixers negligibly affects loop performance, it can be shown from Eq. (16) that

$$(17)\qquad s_{0x}^{m} = \frac{\sqrt{E_{hp}}}{\Delta\omega T_{hp}}\,\sin(\Delta\omega t+\alpha-\beta)\Big|_{mT_r-T_{hp}}^{mT_r}$$

where E_{hp} represents the energy contained in one-half of a signal pulse, i.e.,

$$(18)\qquad E_{hp} \triangleq P_r\,T_{hp}\ ,$$

and $\Delta\omega$ is defined as

$$(19)\qquad \Delta\omega \triangleq \omega_r-\omega_\ell\ .$$

Evaluating Eq. (17) gives the result

$$(20)\qquad s_{0x}^{m} = S\cos\Gamma_0^m$$

where

$$(21)\qquad S \triangleq \sqrt{E_{hp}}\,\frac{\sin(\Delta\omega T_{hp}/2)}{(\Delta\omega T_{hp}/2)}$$

and

$$(22)\qquad \Gamma_0^m \triangleq \Delta\omega[mT_r-(T_{hp}/2)]+\alpha-\beta\ .$$

Similarly, it can be shown that

$$s_{0y}^{m} = S \sin \Gamma_{0}^{m} \quad , \tag{23}$$

$$s_{1x}^{m} = S \cos \Gamma_{1}^{m} \quad , \tag{24}$$

and

$$s_{1y}^{m} = S \sin \Gamma_{1}^{m} \tag{25}$$

where

$$\Gamma_{1}^{m} = \Gamma_{0}^{m} + \Delta\omega T_{hp} \quad . \tag{26}$$

It is clear from Eqs. (20) and (23) that s_{0x}^{m} and s_{0y}^{m} can be interpreted as the components of a two-dimensional vector. That is, Eqs. (20) and (23) are consistent with defining a signal "vector" for each value of m as

$$\underline{S}_{0}^{m} \triangleq s_{0x}^{m} \underline{a}_{x} \; s_{0y}^{m} \underline{a}_{y} \tag{27}$$

where $\underline{a}_{x}$ and $\underline{a}_{y}$ represent orthogonal unit vectors which are aligned with the x and y axes of a right-handed rectangular coordinate frame, respectively. Similarly, $\underline{S}_{1}^{m}$ is defined as

$$\underline{S}_{1}^{m} \triangleq s_{1x}^{m} \underline{a}_{x} + s_{1y}^{m} \underline{a}_{y} \quad . \tag{28}$$

These vectors, i.e., $\underline{S}_{0}^{m}$ and $\underline{S}_{1}^{m}$, each have a magnitude equal to L where

$$L = |S| = \sqrt{E_{hp}} \left| \frac{\sin(\Delta\omega T_{hp}/2)}{\Delta\omega T_{hp}/2} \right| \tag{29}$$

It is obvious from Eqs. (20), (21), and (23) that the angle between $\underline{S}_0^m$ and unit vector $\underline{a}_x$ is given by*

$$(30) \qquad \angle [\underline{S}_0^m, \underline{a}_x] = \begin{cases} \Gamma_0^m & ; \ S > 0 \\ \Gamma_0^m + \pi & ; \ S < 0 \end{cases}$$

and, from Eqs. (21), (24), and (25), that

$$(31) \qquad \angle [\underline{S}_1^m, \underline{a}_x] = \begin{cases} \Gamma_1^m & ; \ S > 0 \\ \Gamma_1^m + \pi & ; \ S < 0 \end{cases} .$$

The angle between vectors $\underline{S}_1^m$ and $\underline{S}_0^m$ is designated by Γ_Δ^m and is given by

$$(32) \qquad \Gamma_\Delta^m \triangleq \angle [\underline{S}_1^m, \underline{S}_0^m] = \Gamma_1^m - \Gamma_0^m = \Delta\omega \ T_{hp}$$

irrespective of the sign of S. Except for an explicable sign difference, this result was obtained by Miller[5] in the process of determining the effect of a frequency offset on the bit error probability performance of a differential detector.

When T_{hp} is fixed at any finite positive value, Eq. (32) assigns a unique value to the angle between the signal vectors for any value of $\Delta\omega$. However, if vectors $\underline{S}_0^m$ and $\underline{S}_1^m$ are given, the angle between them can be assigned an explicit value only if a range of values for that angle which spans 2π radians is prespecified. In this thesis, angles

---

*The notation $\angle[\underline{X},\underline{Y}]$ is employed to designate the angle by which vector $\underline{Y}$ would have to be rotated in a counter clockwise direction to effect alignment with vector $\underline{X}$.

which cannot be assigned explicit values unless a range of values is prespecified are assigned values in the range from minus π to plus π. These values are designated as principal values and are generally represented by lower-case Greek letters. For example, the principal value of Γ_Δ^m, $\{\Gamma_\Delta^m\}_{pv}$, is represented by γ_Δ^m, i.e.

$$\gamma_\Delta^m \triangleq \{\Gamma_\Delta^m\}_{pv} \triangleq \Gamma_\Delta^m - k \cdot 2\pi \tag{33}$$

where k is an integer or zero chosen so that $-\pi < \gamma_\Delta^m \leq \pi$. Since Γ_Δ^m equals $\Delta\omega\ T_{hp}$, angle γ_Δ^m equals zero when $\Delta\omega$ equals zero, the desired value, or when $\Delta\omega$ equals $k \cdot 2\pi/T_{hp}$ where k is an integer (not zero). Thus, if estimates of angle γ_Δ^m for successive values of m are employed as a basis for correcting the local oscillator frequency as in HFTLs of the type considered herein, then the frequency-error estimate can equal zero when frequency offset $\Delta\omega$ equals $k \cdot 2\pi/T_{hp}$. This condition is referred to as a false lock and can occur if the initial frequency offset is sufficiently large or as a result of noise being present at the input to the loop. From Eq. (29), it is seen that the amplitudes of the signal vectors equal zero when $\Delta\omega$ equals $k \cdot 2\pi/T_{hp}$. This fact can be employed as a basis for identifying and correcting false locks. Unless otherwise noted, it is subsequently presumed that the HFTL operates to maintain $\Delta\omega$ at a value much smaller than $2\pi/T_{hp}$ most of the time.

Now, define composite signal vectors $\underline{Z}_0^m$ and $\underline{Z}_1^m$ as

$$\underline{Z}_n^m \triangleq Z_{nx}^m\, \underline{a}_x + Z_{ny}^m\, \underline{a}_y \quad ; \quad n = 0,1 \qquad . \tag{34}$$

The magnitudes of these vectors are represented as

(35) $$Z_n^m \triangleq |\underline{Z}_n^m| \quad ; \quad n = 0,1 \quad .$$

It is easily shown that the composite signal vectors can be represented as

(36) $$\underline{Z}_n^m = \underline{S}_n^m + n_{nx}^m \, \underline{a}_x + n_{ny}^m \, \underline{a}_y \quad ; \quad \text{subscript } n = 0,1 \quad .$$

The angles between vectors $\underline{Z}_n^m$ and associated signal vectors $\underline{S}_n^m$ are designated by ψ_n^m, i.e.,

(37) $$\psi_n^m \triangleq \angle[\underline{Z}_n^m, \underline{S}_n^m] \quad ; \quad n = 0,1 \ ,$$

and are defined so that $-\pi < \psi_n^m \leq \pi$. The angle between $\underline{Z}_1^m$ and $\underline{Z}_0^m$ is defined as θ^m and is given by

(38) $$\theta^m \triangleq \angle[\underline{Z}_1^m, \underline{Z}_0^m] = \Gamma_\Delta^m + \Psi_\Delta^m$$

where

(39) $$\Psi_\Delta^m \triangleq \psi_1^m - \psi_0^m \quad .$$

That is,

(40) $$\theta^m = \Delta\omega \, T_{hp} + \psi_1^m - \psi_0^m \quad .$$

The principal value of θ^m is designated as θ^m:

(41) $$\theta^m \triangleq \{\theta^m\}_{pv} \triangleq \theta^m - k \cdot 2\pi$$

where k is an integer or zero chosen so that $-\pi < \theta^m \leq \pi$.

A visual representation of several vectors and angles which have been defined to this point is given in Fig. 4. In this figure, angles γ_0^m

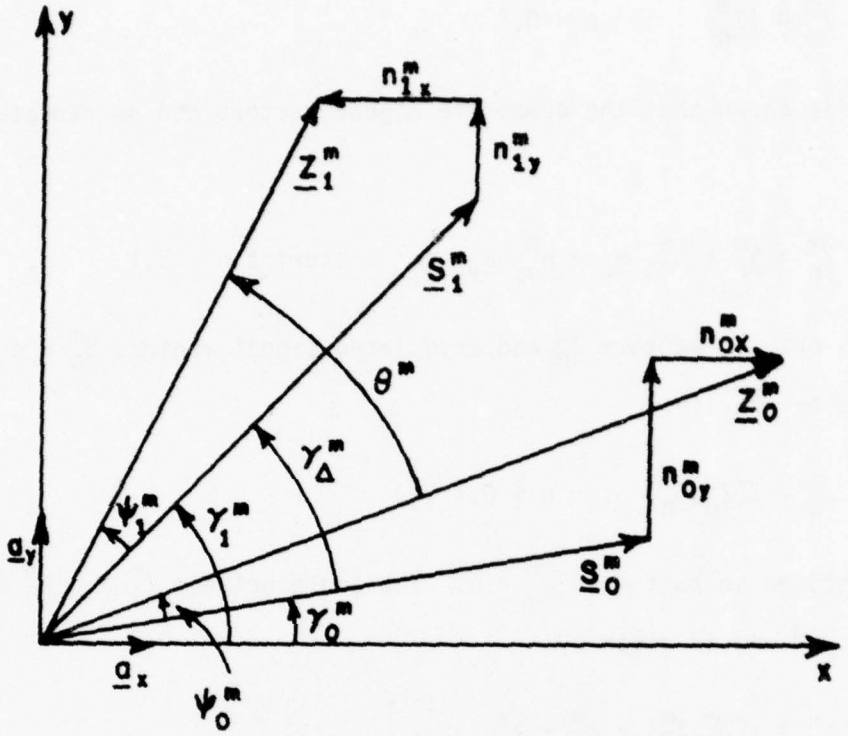

Fig. 4. Received signal vectors in the x,y coordinate frame.

and γ^m_1 represent principal values of angles Γ^m_0 and Γ^m_1, respectively, and are illustrated in a manner which is appropriate when S is positive (see Eqs. (30) and (31)).

Sample voltages Z^m_{0x}, Z^m_{0y}, Z^m_{1x}, and Z^m_{1y} are digitized and input to a digital processor in time sequence (see Figs. 1 and 3). As is shown in Chapter IV, each set of (digitized) sampled voltages can be processed in either of several different ways to generate a suitable estimate of

radian frequency error $\Delta\omega$.* However, for each of the processing algorithms considered, the frequency error estimate is a function of angle θ^m. When the HFTL is operating in the intended manner, the magnitude of angle θ^m is less than π almost all the time and, thus,

$$\theta^m = \Theta^m = \Delta\omega\, T_{hp} + \psi_1^m - \psi_0^m \tag{42}$$

almost all the time. Clearly, the accuracy, with which $\Delta\omega$ can be estimated is dependent on the properties of $\psi_1^m - \psi_0^m$.

Expressions for conditional probability density functions associated with ψ_0^m and ψ_1^m are now derived. To this end, consider $\underline{S}_0^m$ to be given and assume for explicitness that S is positive.** Introduce a second rectangular coordinate frame having axes x' and y' oriented so that axis x' is aligned with vector $\underline{S}_0^m$ as shown in Fig. 5. The projections of vector $\underline{Z}_0^m$ on the x' and y' axes, respectively, are given by

$$Z_{0x'}^m = L + n_{0x'}^m \tag{43}$$

and

$$Z_{0y'}^m = n_{0y'}^m \tag{44}$$

where

$$n_{0x'}^m = (\cos \gamma_0^m) n_{0x}^m + (\sin \gamma_0^m) n_{0y}^m \tag{45}$$

---

* It is assumed that the quantization error introduced by the digital subsystem is negligibly small.

** The discussion can be made applicable to the case where S is negative by replacing γ_0^m with $\gamma_0^m + \pi$.

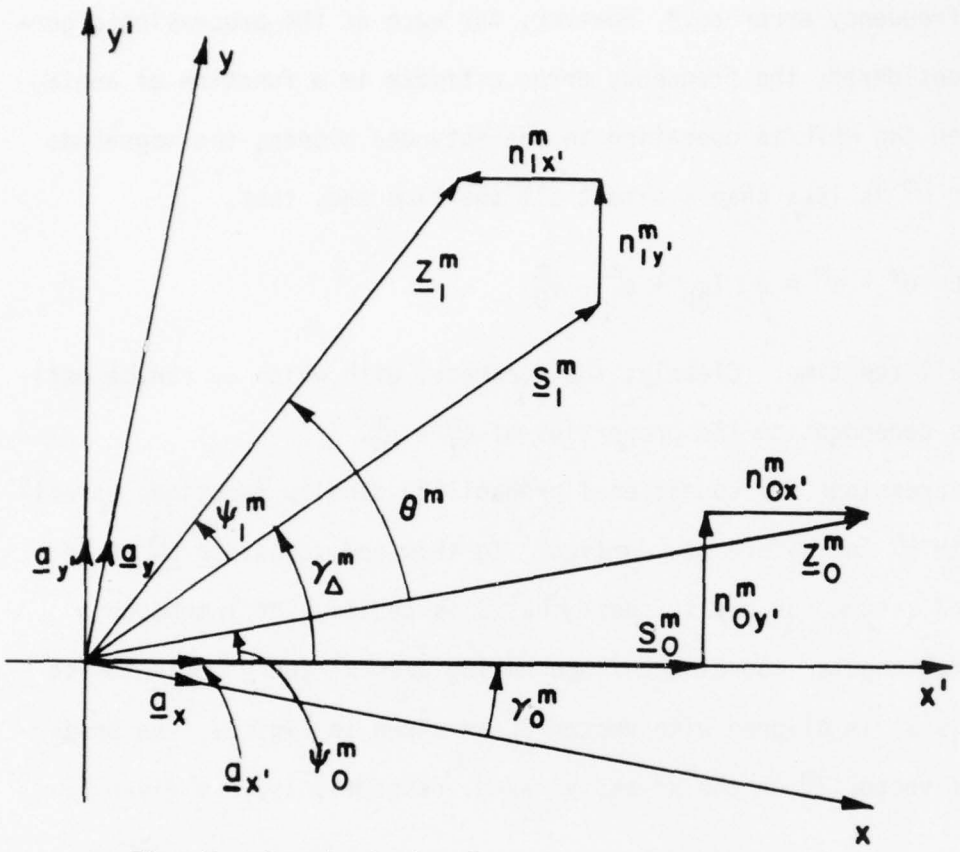

Fig. 5. Received signal vectors in the x',y' coordinate frame.

and

$$n^m_{0y'} = -(\sin \gamma^m_0) n^m_{0x} + (\cos \gamma^m_0) n^m_{0y} \quad . \tag{46}$$

Further, the projections of $\underline{Z}^m_1$ on the x' and y' axes, respectively, are given by

$$Z^m_{1x'} = L \cos(\Delta\omega \, T_{hp}) + n^m_{1x'} \tag{47}$$

and

(48) $$Z^m_{1y'} = L \cos(\Delta\omega\, T_{hp}) + n^m_{1y'}$$

where

(49) $$n^m_{1x'} = (\cos \gamma^m_0) n^m_{1x} + (\sin \gamma^m_0) n^m_{1y}$$

and

(50) $$n^m_{1y'} = -(\sin \gamma^m_0) n^m_{1x} + (\cos \gamma^m_0) n^m_{1y} \quad .$$

As previously noted, n^m_{0x}, n^m_{0y}, n^m_{1x}, and n^m_{1y} are sample sequences from independent zero-mean Gaussian sequences which each have a variance of $N_o/2$. For this case, it can be shown that n^m_{0x}, n^m_{0y}, n^m_{1x}, and n^m_{1y} are also sample sequences from independent zero-mean Gaussian sequences which each have a variance of $N_o/2$[6]. Consequently, the conditional joint density function $p(Z^m_{0x'}, Z^m_{0y'}/L)$ is given by

(51) $$p(Z^m_{0x'}, Z^m_{0y'}/L) = \frac{1}{\pi N_o} \exp\left[- \frac{(Z^m_{0x'} - L)^2 + (Z^m_{0y'})^2}{N_o} \right] \quad .$$

Using this result and the transformation

(52) $$Z^m_{0x'} = Z^m_0 \cos \psi^m_0$$

(53) $$Z^m_{0y'} = Z^m_0 \sin \psi^m_0$$

an expression for the conditional joint density function $p(Z^m_0, \psi^m_0/L)$ can be derived. In turn, this expression can be integrated (4) over Z^m_0 to yield

$$(54) \qquad p(\psi_0^m/L) = \frac{1}{2\pi} \exp\left[-\frac{L^2}{N_o}\right] + \frac{1}{\sqrt{2\pi}} \exp\left[-\frac{L^2 \sin^2 \psi_0^m}{N_o}\right]$$

$$\cdot L\sqrt{\frac{2}{N_o}} (\cos \psi_0^m) \left[\frac{1}{2} + \frac{1}{\sqrt{2\pi}} \int_0^{L\sqrt{2/N_o} \cos\psi_0^m} \exp\left(-\frac{u^2}{2}\right) du\right] \quad .$$

Similarly, it can be shown that substituting ψ_1^m for ψ_0^m in Eq. (54) gives the correct expression for $p(\psi_1^m/L)$. These results will be employed as a partial basis for developing an approximate linear model for the HFTL in Chapter III.

The frequency of the D-C/VFO in the HFTL is presumed to be expressible in the equivalent form

$$(55) \qquad \omega_\ell = \omega_o + K_v e_c$$

where e_c represents an analog equivalent of the digital control word, K_v represents the VFO gain in radians per second per volt, and ω_o represents the radian frequency of the VFO output signal when e_c equals zero: the "rest" frequency. Control voltage e_c is presumed to be generated by incrementing its value following the processing of each received pulse by an amount proportional to the frequency error estimate. For convenience of subsequent discussion, differential radian frequencies are defined as

$$(56) \qquad \delta\omega_r \triangleq \omega_r - \omega_o$$

and

(57) $$\delta\omega_\ell \triangleq \omega_\ell - \omega_o = K_v\, e_c \quad .$$

The difference between these differential frequencies is the same as the difference between the actual frequencies, i.e.,

(58) $$\delta\omega_r - \delta\omega_\ell = \omega_r - \omega_o - (\omega_\ell - \omega_o) = \omega_r - \omega_\ell = \Delta\omega \quad .$$

The development of exact expressions in closed form which characterize the effects of noise on loop performance is unmanagably difficult. Thus, resort to approximate analyses and simulations via digital computation is necessary to obtain useful results. These approaches are pursued in the following two chapters.

CHAPTER III

APPROXIMATE LINEAR MODELING AND ANALYSIS

An approximate expression for the standard deviation of the HFTL frequency tracking error due to noise is derived in this chapter. First, results presented in the preceding chapter are employed to develop an approximate linear model of the HFTL. Approximate linear analyses are then performed to obtain the result of interest.

Two characteristics of the HFTL virtually preclude the development of exact expressions which describe the effects of noise on loop perfromance: 1) for given values of the sample noise voltages, the values of phase noises ψ_0^m and ψ_1^m depend on the value of L which, in turn, depends on the radian frequency error $\Delta\omega$ (see Eq. (29)) and 2) the observable angle θ^m equals the angle being estimated, Θ^m, only when the magnitude of the latter angle is less than π. In this chapter, the obstacles presented by those characteristics are avoided by assuming that the half-pulse energy to single-sided noise spectral density ratio, E_{hp}/N_o, is sufficiently large so that angles $\Delta\omega\ T_{hp}$, ψ_0^m, and ψ_1^m are each much smaller than one radian most of the time and that Θ^m is an observable angle irrespective of its value. When E_{hp}/N_o is sufficiently large, it can be shown from Eq. (54) that angle ψ_0^m is very nearly Gaussian distributed with a mean value of zero and a variance of $(N_o/2E_{hp})$:

$$\sigma^2_{\psi_0^m} \cong \frac{N_o}{2E_{hp}} \quad . \tag{59}$$

Since ψ_0^m and ψ_1^m are identically distributed, independent, and (nearly) Gaussian processes when E_{hp}/N_o is sufficiently large, process ψ_Δ^m (which equals $\psi_1^m - \psi_0^m$) is also nearly Gaussian distributed with a mean value of a zero a variance of N_o/E_{hp}:

$$\sigma^2_{\psi_\Delta^m} \cong \frac{N_o}{E_{hp}} \quad . \tag{60}$$

A linear model of the HFTL which is consistent with all foregoing results when E_{hp}/N_o is sufficiently large is given in Fig. 6. As shown in this figure, the "processor" which generates control voltage e_c is modeled by an ideal impulse sampler and an integrator having a gain equal to G_p. Each "new" value of e_c is made available to an ideal

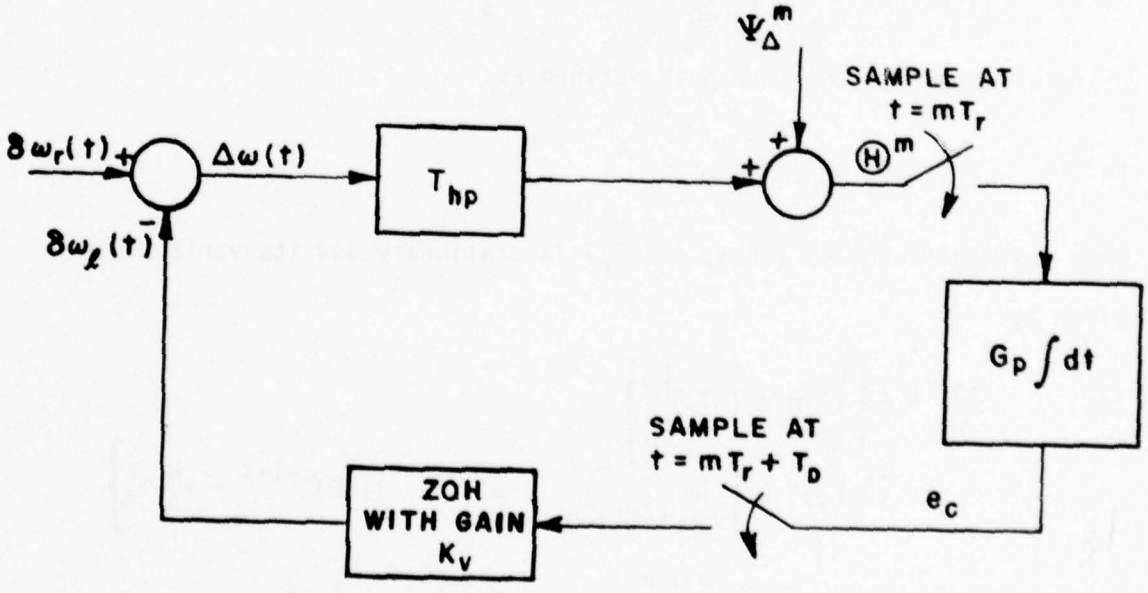

Fig. 6. A linear model of the hybrid frequency tracking loop.

zero-order hold circuit which has a gain equal to K_v by a "second" sampler. The sampling instants of this second sampler are delayed by a processing time T_D with respect to the sampling instants of the "first" sampler.

The manner in which phase noise ψ_Δ^m affects the mean and standard deviation of radian frequency error $\Delta\omega$ is now determined for the case where differential radian frequency $\delta\omega_r$ is equal to a constant. Clearly, the mean value of the frequency tracking error due to noise equals zero since ψ_Δ^m has a mean value of zero and the loop model is linear (in a sampled-data sense). The variance of the radian frequency tracking error due to noise is calculated by first assuming that $\Delta\omega$ equals zero at time t equal to zero. For this case, it can be shown that the radian frequency error at time t equal to mT_r is given by [7]

$$\Delta\omega(mT_r) = - G_p K_v \sum_{k=0}^{m-1} (1-G)^{m-1-k} \psi_\Delta^k \quad ; \quad m = 1,2,\cdots \tag{61}$$

where G represents the loop gain defined as

$$G \triangleq G_p K_v T_{hp} \quad . \tag{62}$$

When m is sufficiently large, $\Delta\omega(mT_r)$ is stationary and its variance is given by

$$\begin{aligned} \sigma_{\Delta\omega}^2 &\triangleq E\left\{\left[\lim_{m\to\infty} \Delta\omega(mT_r)\right]^2\right\} \\ &= (G_p K_v)^2 \, E\left\{\lim_{m\to\infty} \sum_{k=0}^{m-1} \sum_{\ell=0}^{m-1} (1-G)^{m-1-k} \, (1-G)^{m-1-\ell} \cdot \psi_\Delta^k \, \psi_\Delta^\ell\right\} \\ &= (G_p K_v)^2 \lim_{m\to\infty} \sum_{k=0}^{m-1} \sum_{\ell=0}^{m-1} (1-G)^{2m-2-k-\ell} \, E\{\psi_\Delta^k \, \psi_\Delta^\ell\} \end{aligned} \tag{63}$$

where E{x} designates the expected value of x.

Now, ψ_Δ^k and ψ_Δ^ℓ are clearly independent when $k \neq \ell$, i.e.,

$$E\{\psi_\Delta^k \psi_\Delta^\ell\} = 0 \quad ; \quad k \neq \ell \qquad . \tag{64}$$

By definition

$$E\{(\psi_\Delta^k)^2\} \triangleq \sigma^2_{\psi_\Delta^m} \qquad . \tag{65}$$

Employing these latter equations to evaluate Eq. (63) gives

$$\sigma^2_{\Delta\omega} = (G_p K_v)^2 \, \sigma^2_{\psi_\Delta^m} \lim_{m\to\infty} \sum_{k=0}^{m-1} [(1-G)^2]^k \tag{66}$$

$$= \frac{(G_p K_v)^2}{G(2-G)} \; \sigma^2_{\psi_\Delta^m} \quad ; \quad 0 < G < 2 \qquad .$$

It can be shown through a joint use of this result and Eqs. (60) and (62) that $\sigma_{\Delta\omega}$ is given by

$$\sigma_{\Delta\omega} = \frac{1}{T_{hp}} \left(\frac{G}{2-G}\right)^{1/2} \left(\frac{E_{hp}}{N_o}\right)^{-1/2} \qquad . \tag{67}$$

A dimensionless frequency ratio is now defined as

$$\rho \triangleq \frac{\Delta f}{1/T_{hp}} = \frac{\Delta\omega}{2\pi} \; T_{hp} \qquad . \tag{68}$$

The standard deviation of ρ is given by

$$\sigma_\rho = \frac{1}{2\pi} \left(\frac{G}{2-G}\right)^{1/2} \left(\frac{E_{hp}}{N_o}\right)^{-1/2} \qquad . \tag{69}$$

This expression was employed to generate graphs of σ_ρ versus E_{hp}/N_o for several values of loop gain G. These graphs and numerical results obtained by simulating the HFTL on a digital computer are presented jointly in the following chapter.

CHAPTER IV

COMPUTER-IMPLEMENTED HFTL SIMULATIONS AND NUMERICAL RESULTS

A digital computer was employed to simulate HFTLs having both unavoidable and deliberately-incorporated nonlinearities, and numerical results were obtained which show the effects of the nonlinearities investigated on the standard deviation of frequency ratio ρ (see Eq. (68)). These results are presented in this chapter and are compared with results predicted by Eq. (69). Data descriptive of distribution functions associated with ρ for selected loop configurations and parameter values are also given.

The model of the loop simulated by the computer program developed is shown in Fig. 7. Note that, in this model, differential radian frequency $\delta\omega_r(m)$ is accumulated rather than the control voltage and sample voltages defined relative to the x',y' coordinate frame are generated and processed rather than sample voltages defined relative to the x,y coordinate frame. However, the two models suggested by this statement are mathematically equivalent for the estimator algorithms to be considered. A listing of the simulation program is given in Appendix A.

At the beginning of each program run, the differential L.O. frequency was set equal to zero and the differential input frequency was fixed at an appropriate value. One-hundred iterations of the program

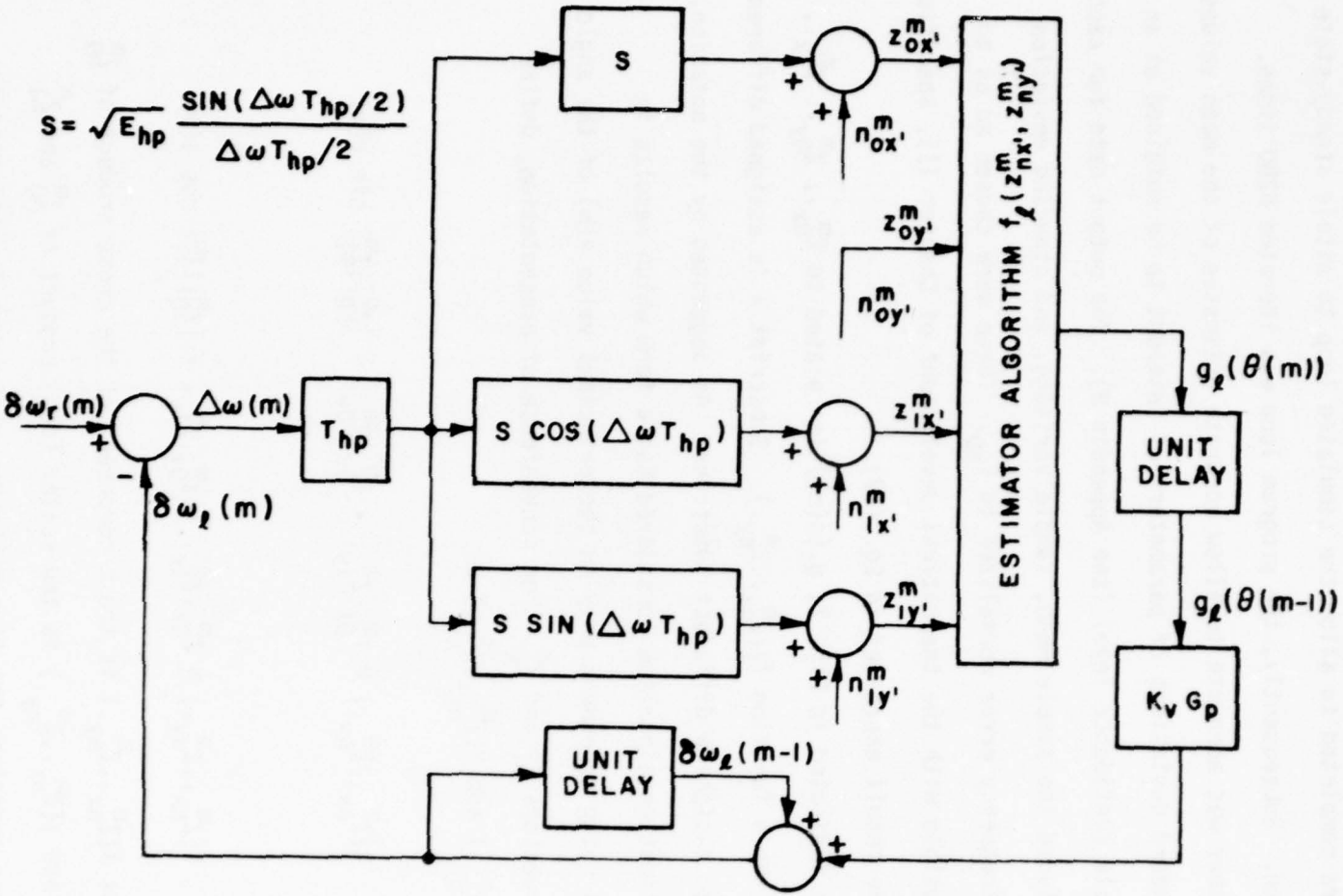

Fig. 7. Model of the hybrid frequency tracking loop simulated on a digital computer.

loop were completed to allow the simulated loop to attain steady-state operation. Subsequently, the program loop was iterated 6200 times. This number was adequate to allow accurate estimates of the mean values and standard deviations of parameters of interest to be obtained at an acceptable confidence level (see Appendix B). The output data for each run included the sample mean, sample variance, and standard deviation of the frequency error normalized to T_{hp}. These were chosen so as to be compatible with the theoretical development of Chapter III, specifically, the result expressed in Eq. (69).

As indicated in Fig. 7, $g_\ell(\theta(m))$ is related to $Z^m_{0x'}$, $Z^m_{0y'}$, $Z^m_{1x'}$, and $Z^m_{1y'}$ by a function $f_\ell(Z^m_{nx'},Z^m_{ny'})$. Subscript ℓ is assigned different values to designate different functions. As suggested by the notation, each estimation algorithm considered has a form which results in $g_\ell(\theta(m))$ being dependent only on the principal value $\theta(m)$ of the angle between vectors $\underline{Z}^m_1$ and $\underline{Z}^m_0$. For convenience of presentation, define $X(Z^m_{nx'},Z^m_{ny'})$ and $Y(Z^m_{nx'},Z^m_{ny'})$ as

$$(70) \qquad X(Z^m_{nx'},Z^m_{ny'}) \triangleq Z^m_{0x'}Z^m_{1y'} - Z^m_{1x'}Z^m_{0y'} = |\underline{Z}^m_0||\underline{Z}^m_1| \sin\theta(m)$$

and

$$(71) \qquad Y(Z^m_{nx'},Z^m_{ny'}) \triangleq Z^m_{0x'}Z^m_{1x'} + Z^m_{0y'}Z^m_{1y'} = |\underline{Z}^m_0||\underline{Z}^m_1| \cos\theta(m) \quad .$$

Note that $X(Z^n_{nx'},Z^m_{ny'})$ is the z component of the cross product of $\underline{Z}^m_0$ and $\underline{Z}^m_1$, and $Y(Z^m_{nx'},Z^m_{ny'})$ is the scalar (dot) product of $\underline{Z}^m_0$ and $\underline{Z}^m_1$. Using this notation, the five estimator algorithms investigated are expressible as follows:

$$(72) \qquad g_1(\theta) = f_1(Z^m_{nx'}, Z^m_{ny'}) = \mathrm{Tan}^{-1}\left[\frac{X(Z^m_{nx'}, Z^m_{ny'})}{Y(Z^m_{nx'}, Z^m_{ny'})}\right]$$

where Tan^{-1} represents a four-quadrant inverse tangent function,

$$(73) \qquad g_2(\theta) = f_2(Z^m_{nx'}, Z^m_{ny'}) = \arctan\left[\frac{X(Z^m_{nx'}, Z^m_{ny'})}{Y(Z^m_{nx'}, Z^m_{ny'})}\right]$$

where arctan represents a two-quadrant inverse tangent function,

$$(74) \qquad g_3(\theta) = f_3(Z^m_{nx'}, Z^m_{ny'}) = \frac{X(Z^m_{nx'}, Z^m_{ny'})}{Y(Z^m_{nx'}, Z^m_{ny'})} = \tan\theta \quad ,$$

$$(75) \qquad g_4(\theta) = f_4(Z^m_{nx'}, Z^m_{ny'}) = \frac{X(Z^m_{nx'}, Z^m_{ny'})}{|Y(Z^m_{nx'}, Z^m_{ny'})|} \quad ,$$

and

$$(76) \qquad g_5(\theta) = f_5(Z^m_{nx'}, Z^m_{ny'}) = \frac{X(Z^m_{nx'}, Z^m_{ny'})}{[X^2(Z^m_{nx'}, Z^m_{ny'}) + Y^2(Z^m_{nx'}, Z^m_{ny'})]^{1/2}}$$

$$= \sin\theta \quad .$$

The functions $g_1(\theta)$ through $g_5(\theta)$ are illustrated in Figs. 8 through 12, respectively.

The standard deviation of frequency ratio ρ is shown plotted as a function of the half-pulse energy to single-sided noise spectral density ratio for each $g_\ell(\theta)$ and for a loop gain equal to one in Fig. 13. Theoretical results generated using Eq. (69) are shown in this figure along with the numerical data obtained. As expected, the numerical data are in close agreement with the analytical result when the value of E_{hp}/N_o is sufficiently large for each $g_\ell(\theta)$. For the $g_1(\theta)$ case, the

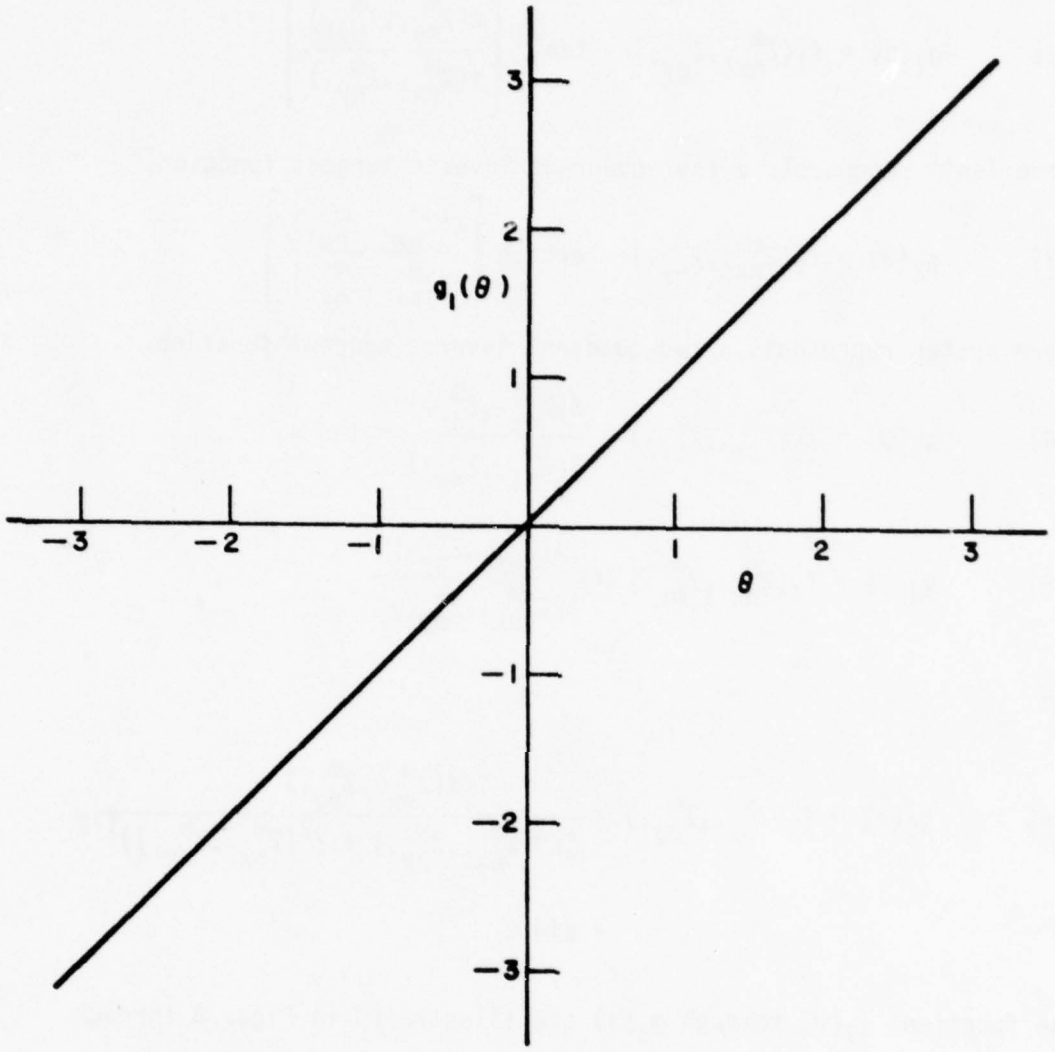

Fig. 8. The linear estimator.

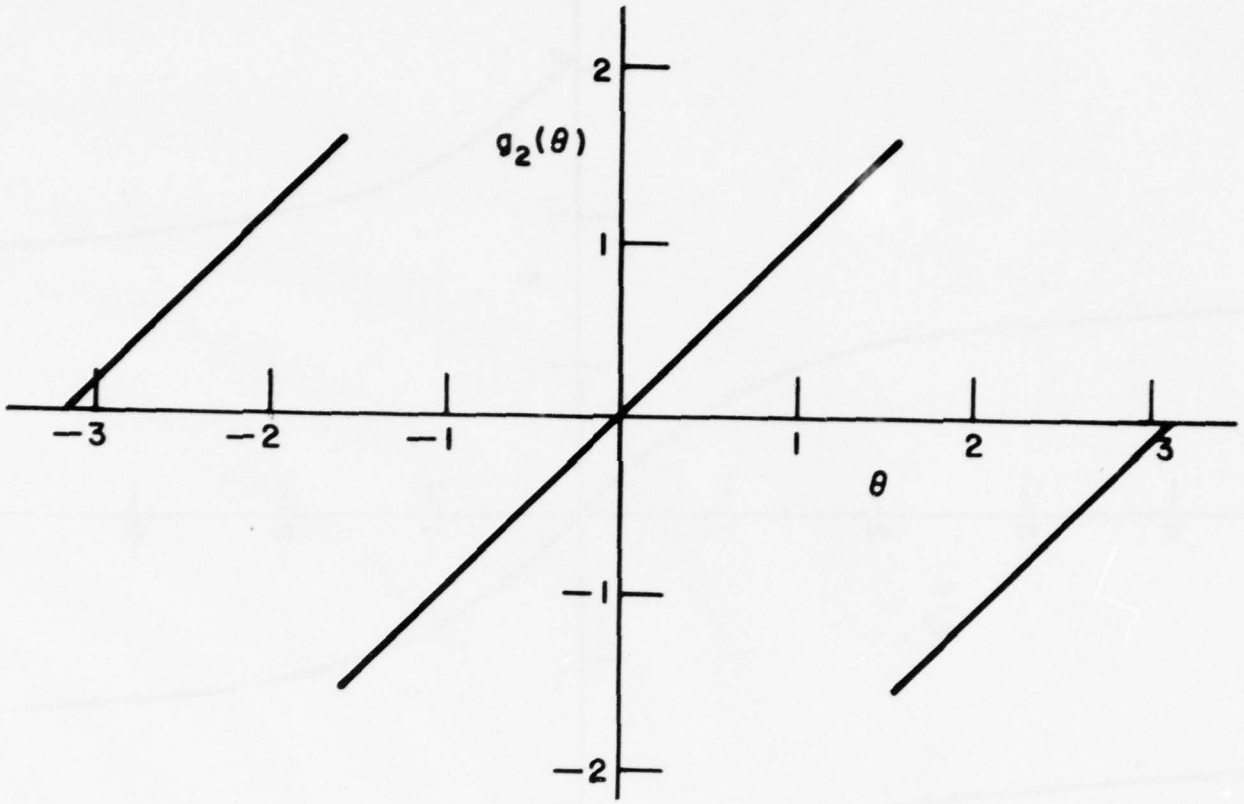

Fig. 9. The linear estimator with decreased look range.

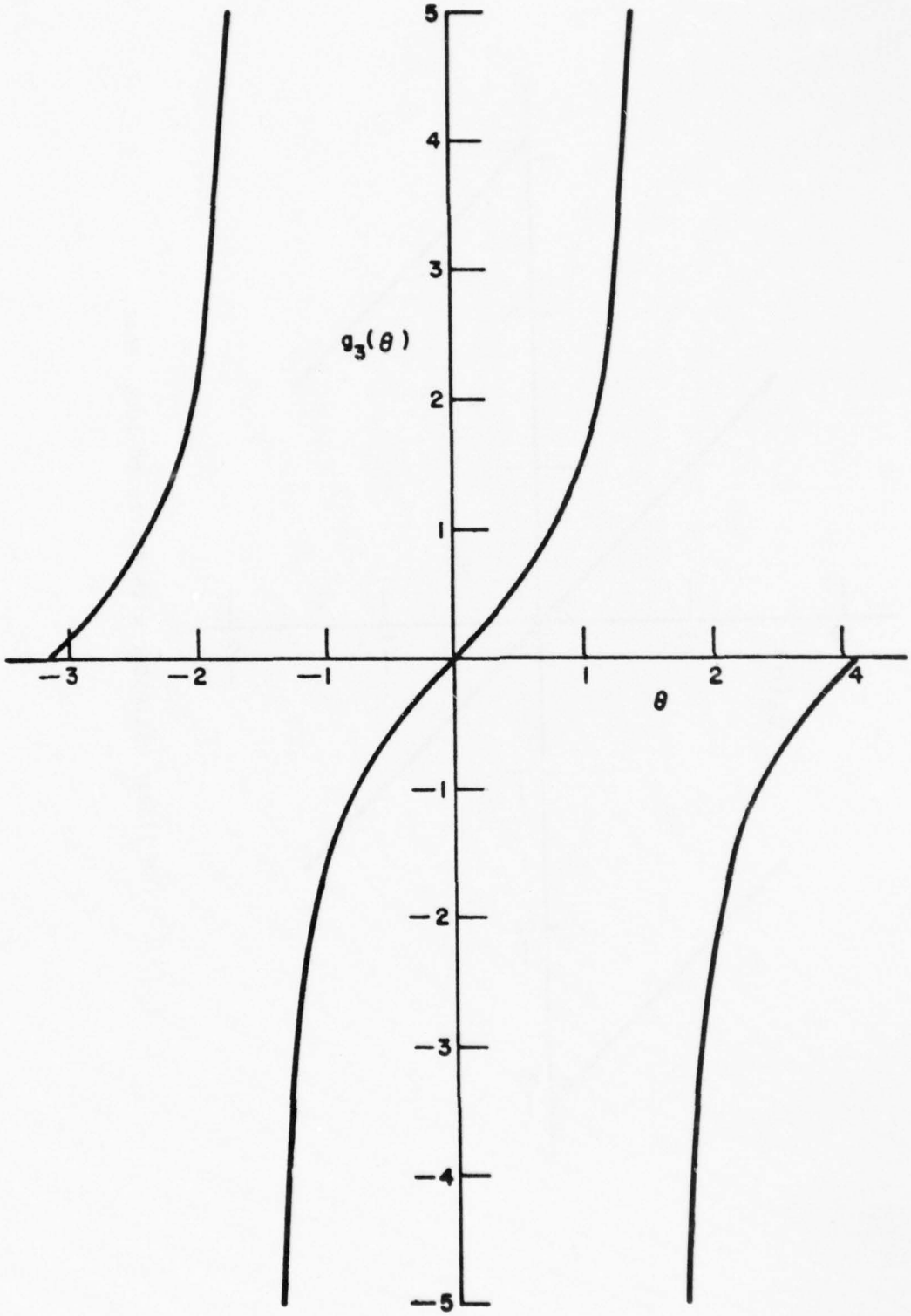

Fig. 10. The tangent estimator.

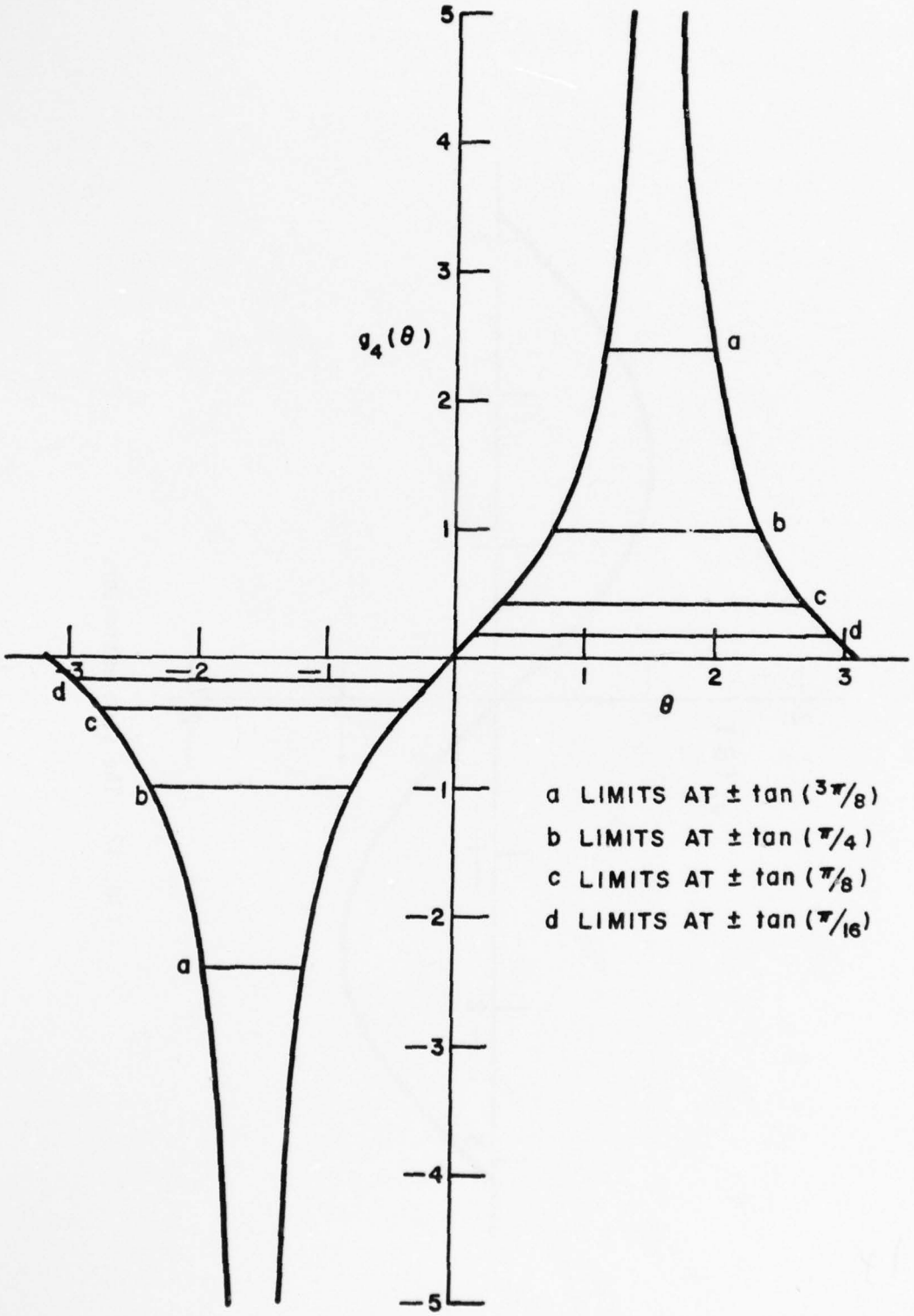

Fig. 11. The modified tangent estimator with increased lock range; four possible limits are shown.

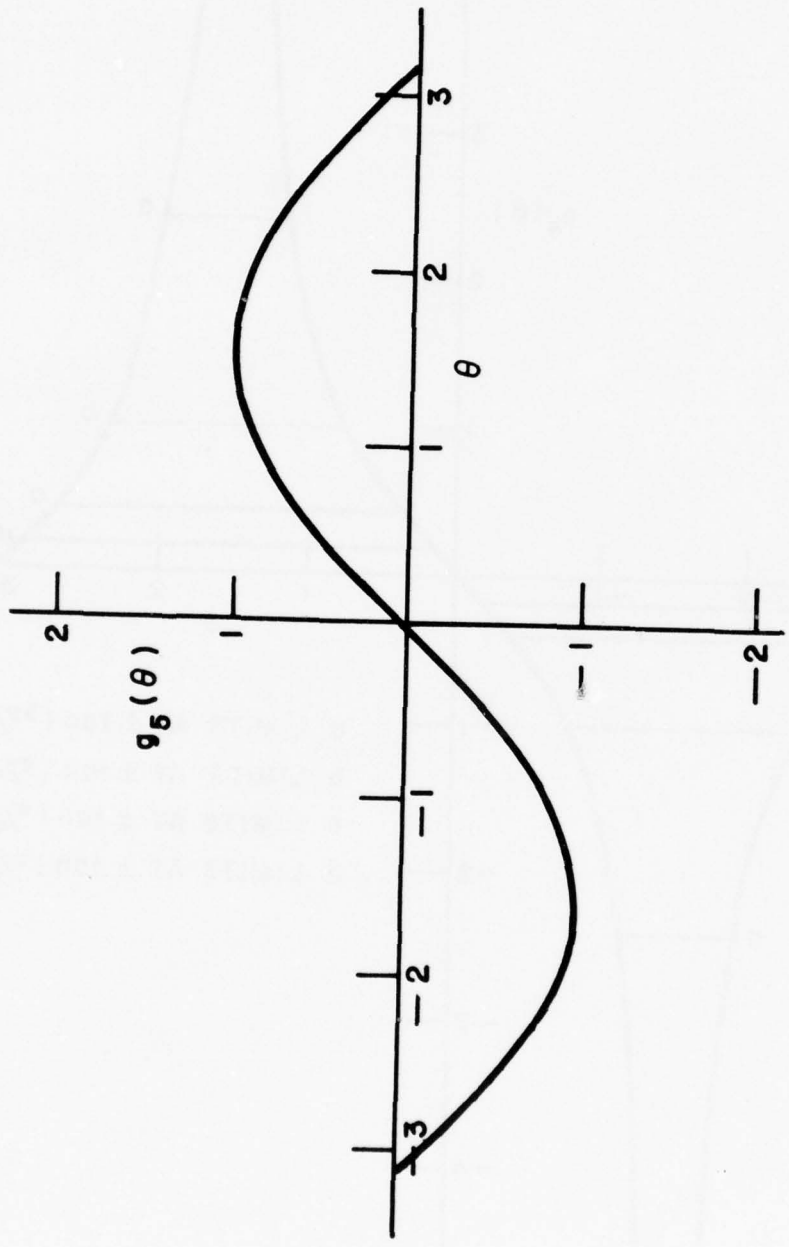

Fig. 12. The sine estimator.

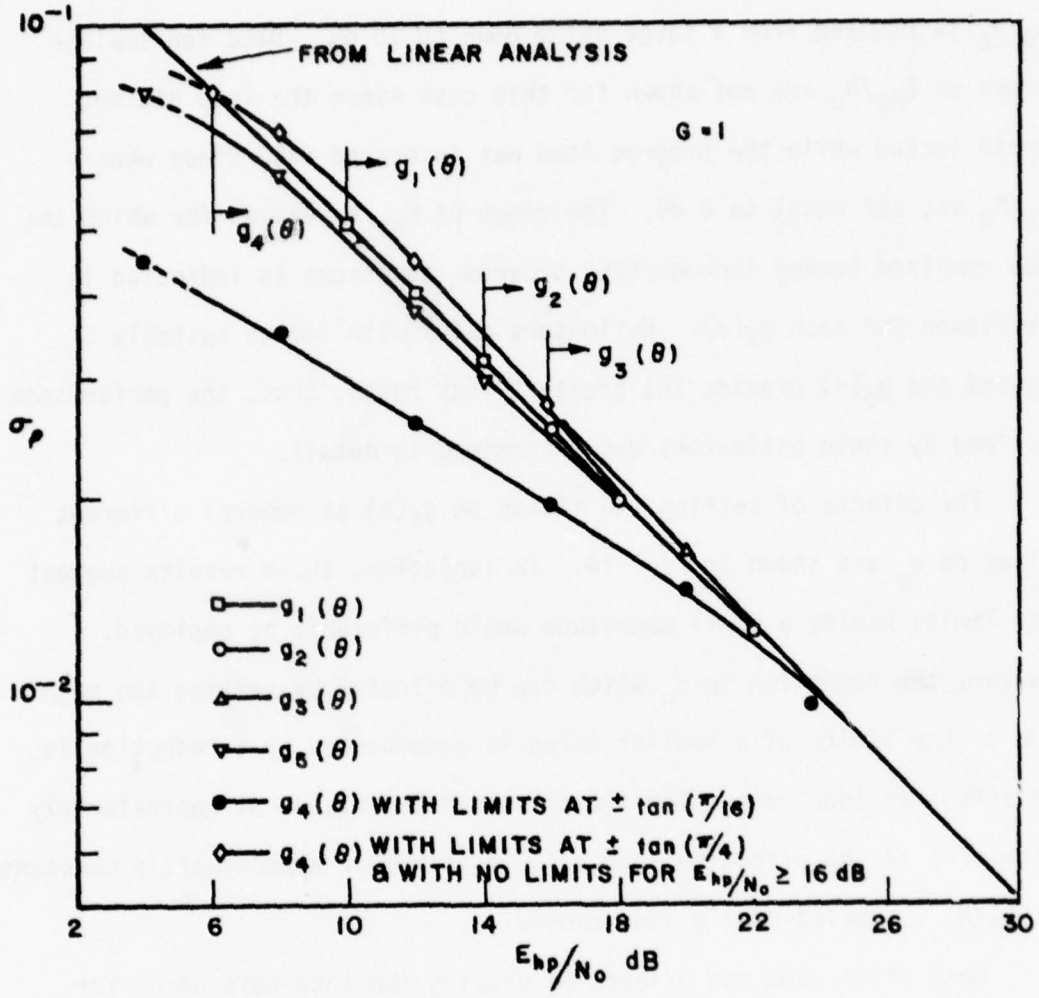

Fig. 13. Standard deviation of the normalized frequency-tracking error versus half pulse energy to single-sided noise spectral density ratio for various estimators and a loop gain equal to one: G=1.

numerical data remain in close agreement with the analytical result as E_{hp}/N_o is reduced from a large value down to 10 dB. Data for smaller values of E_{hp}/N_o are not shown for this case since the loop did not remain locked while the program loop was interated 6200 times when E_{hp}/N_o was set equal to 8 dB. The range of E_{hp}/N_o values for which the loop remained locked through 6200 program iterations is indicated in the figure for each $g_\ell(\theta)$. Estimators $g_4(\theta)$ with limits suitably imposed and $g_5(\theta)$ provide the greatest lock range; thus, the performance provided by these estimators was determined in detail.

The effects of setting the limits on $g_4(\theta)$ at several different values on σ_ρ are shown in Fig. 14. In isolation, these results suggest that limits having a small magnitude would preferably be employed. However, the reduction in σ_ρ which can be effected by setting the magnitude of the limits at a smaller value is accompanied by a reduction in the effective loop gain. The limits should be imposed at approximately $\pm \tan(\pi/4)$ if the effective loop gain is to remain approximately constant as E_{hp}/N_o is varied over a wide range.

Data which show the effects of varying the loop gain on σ_ρ for the $g_4(\theta)$ case with limits set at $\pm \tan(\pi/4)$ and for the $g_5(\theta)$ case are shown in Figs. 15 and 16, respectively. The numerical results are in reasonable agreement with results obtained using Eq. (69)

A subroutine to the simulation program, when called, orders the values of ρ and then calculates the percentage of the samples which have values smaller than a specified value. Thus, the distribution of ρ was readily determinable. Distribution data were obtained for six cases of interest; these data are given in Figs. 17-19. The straight line

associated with each set of points represents a Gaussian distribution with a mean and variance equal to the sample mean and sample variance of the error data. Clearly, the distribution of ρ does not differ markedly from a Gaussian distribution -- even when loop gain G equal 1.25 and E_{hp}/N_o equals 8 dB.

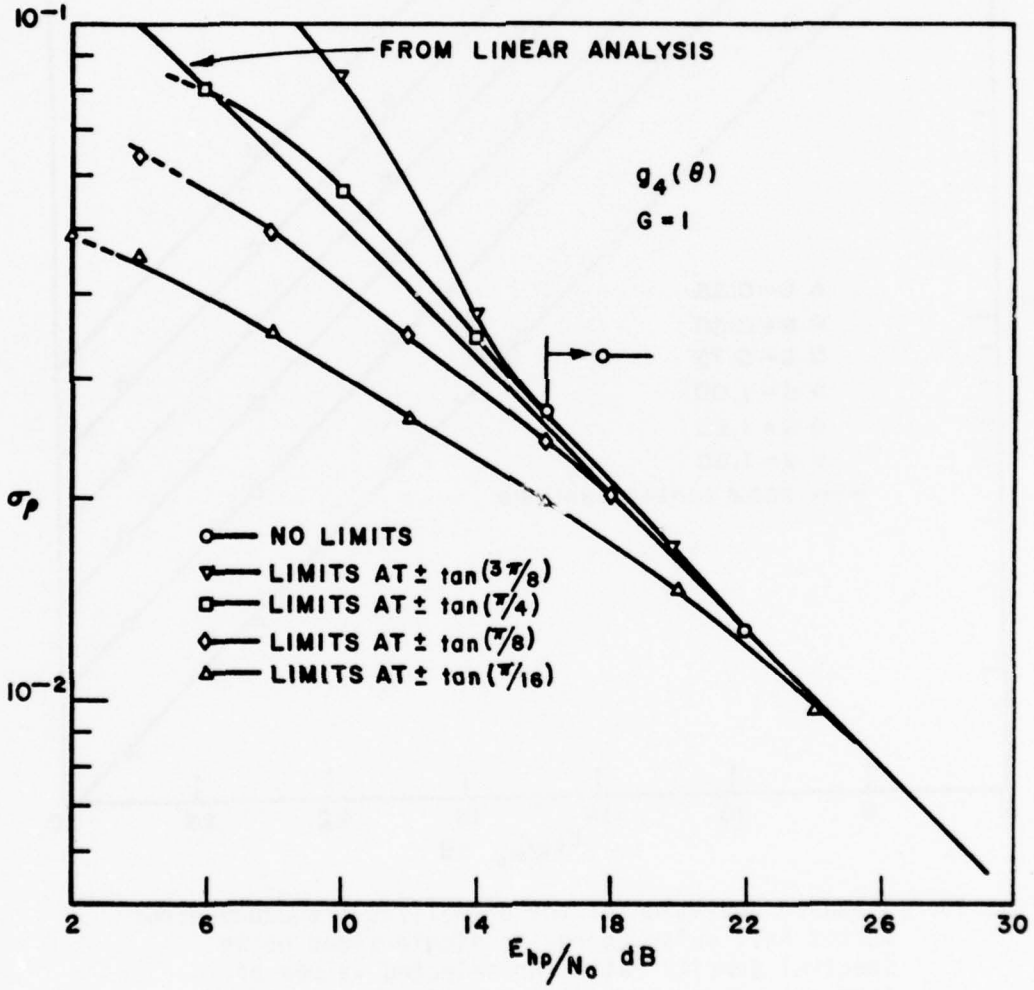

Fig. 14. Standard deviation of the normalized frequency error versus half-pulse energy to single-sided noise spectral density ratio for the modified tangent estimator and a loop gain equal to one: G=1.

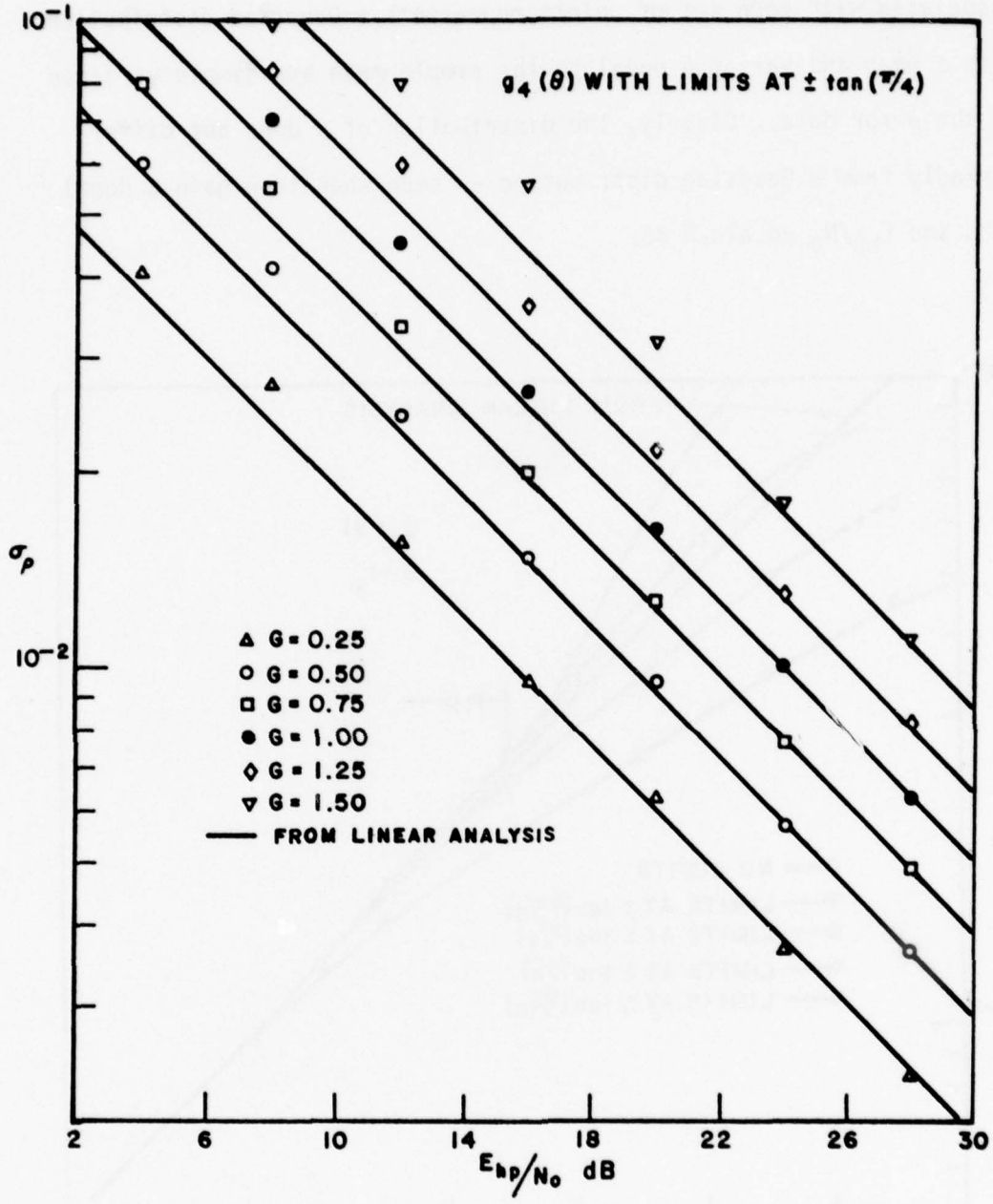

Fig. 15. Standard deviation of the normalized frequency error versus half pulse energy to single-sided noise spectral density ratio for selected values of loop gain when the modified tangent estimator is employed with limits at $\pm\tan(\pi/4)$.

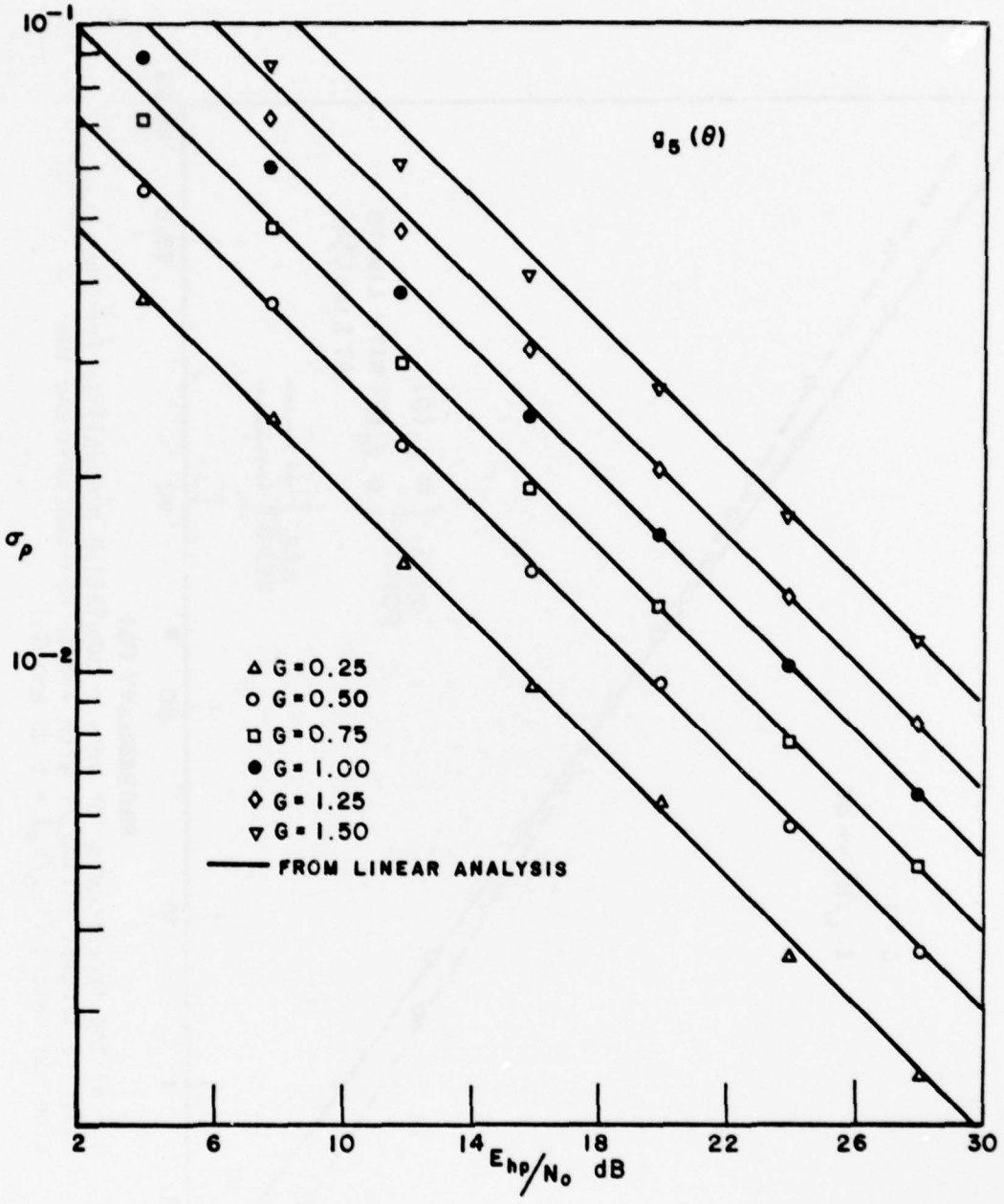

Fig. 16. Standard deviation of the normalized frequency error versus half pulse energy to single-sided noise spectral density ratio for selected values of loop gain when the sine estimator is employed.

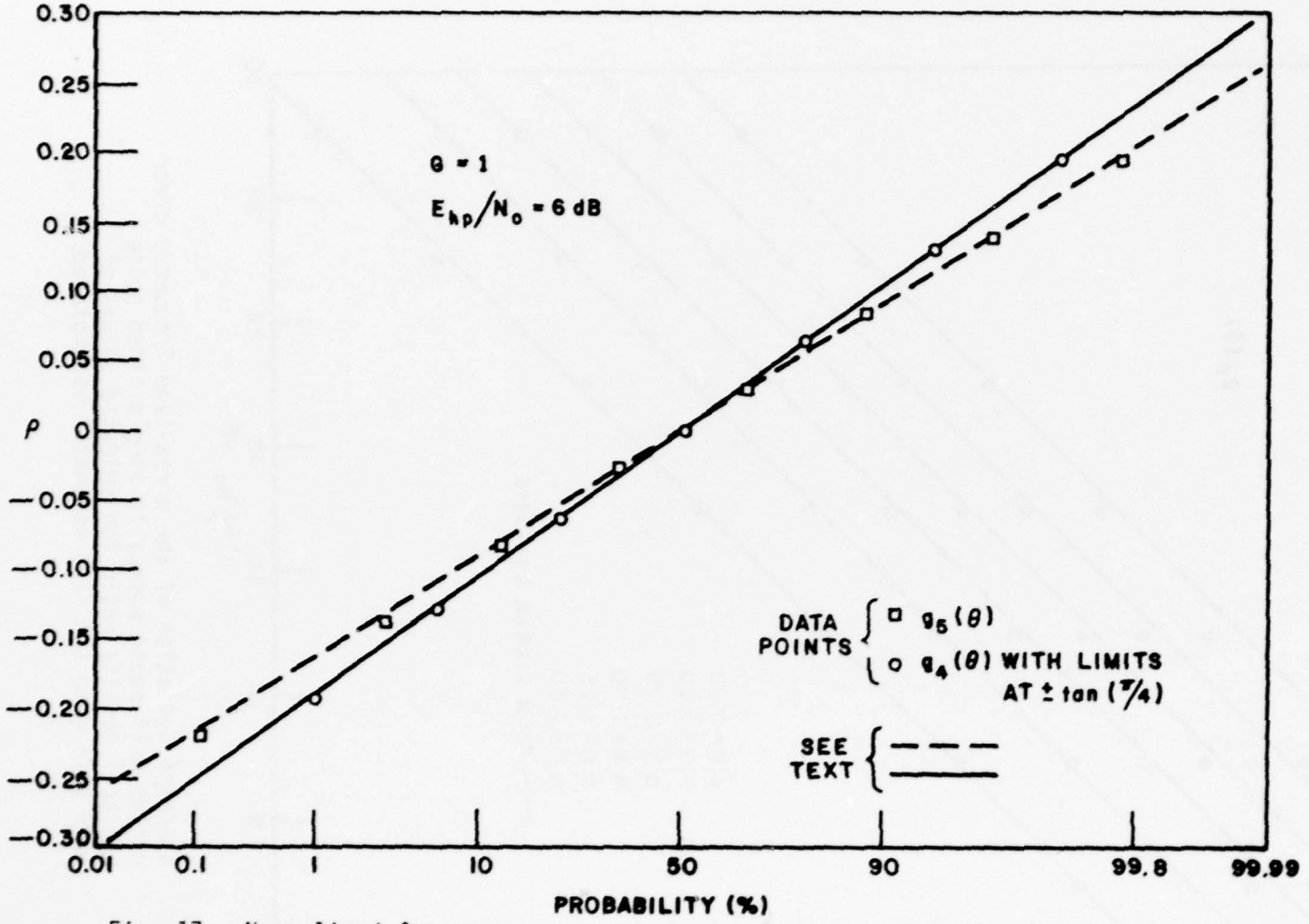

Fig. 17. Normalized frequency error versus cumulative probability for the modified tangent estimator with limits at $\pm\tan(\pi/4)$ and the sine estimator: (E_{hp}/N_o) = 6 dB and G=1.

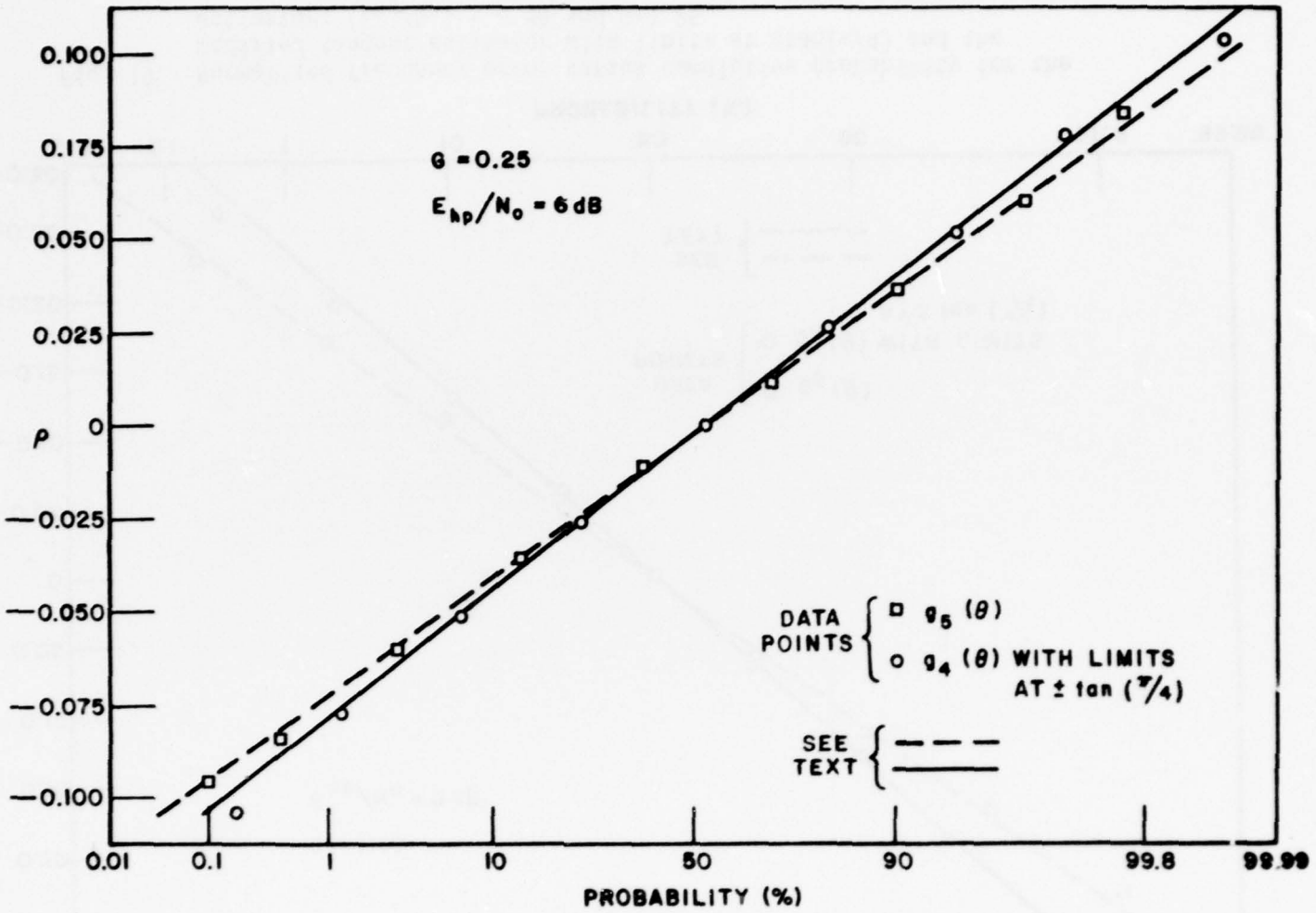

Fig. 18. Normalized frequency error versus cumulative probability for the modified tangent estimator with limits at $\pm\tan(\pi/4)$ and the sine estimator; (E_{hp}/N_0) = 6 dB and G = 0.25.

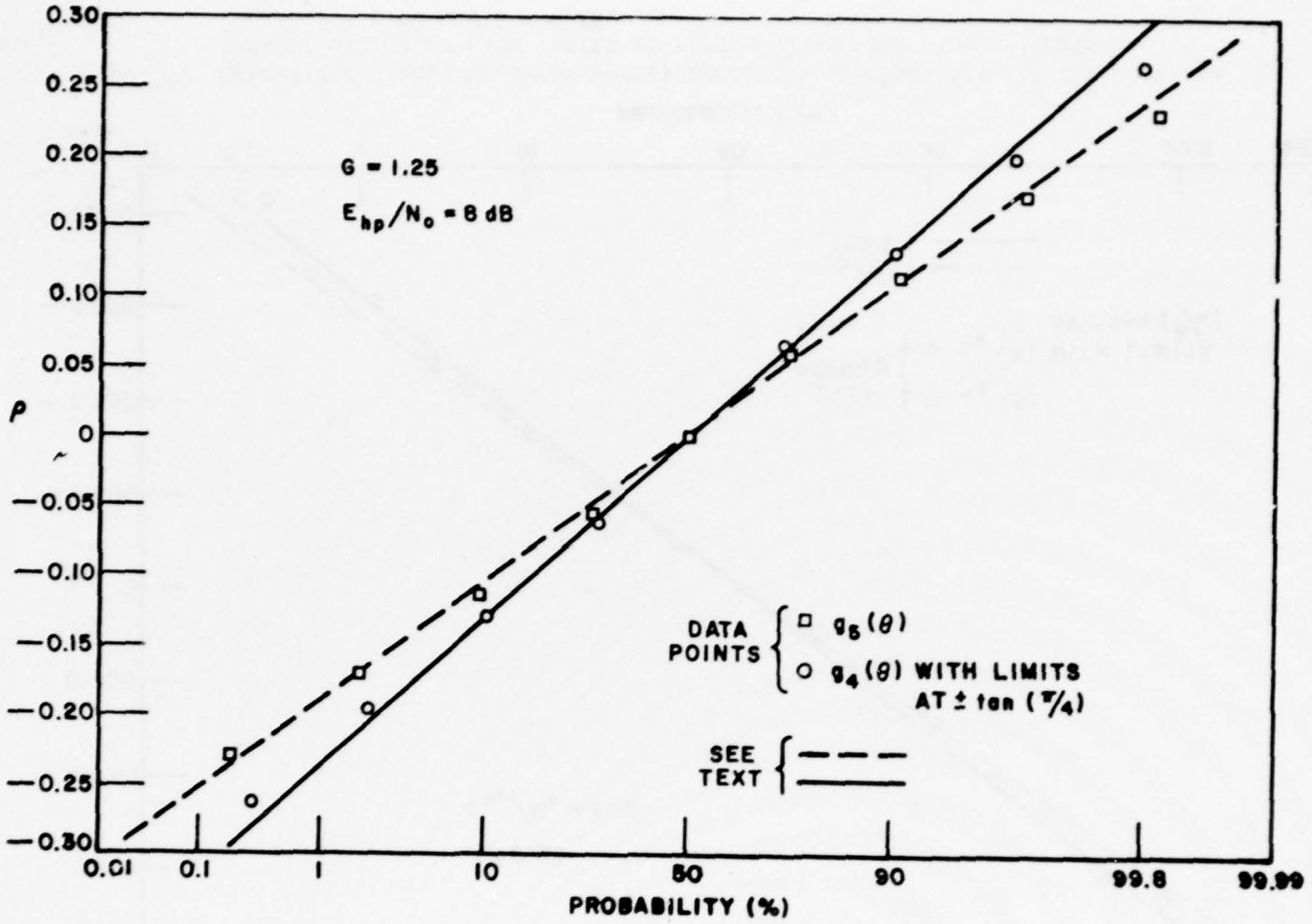

Fig. 19. Normalized frequency error versus cumulative probability for the modified tangent estimator with limits at $\pm\tan(\pi/4)$ and the estimator; (E_{hp}/N_o) = 8 dB and G=1.25.

CHAPTER V

SUMMARY AND CONCLUSIONS

The configuration and performance of a hybrid frequency tracking loop which tracks the frequency of a pulsed sinusoid have been addressed in this thesis. A linear model of the loop was developed and an approximate expression was derived for the standard deviation of the frequency tracking error due to the presence of additive white Gaussian noise at the loop's input. Results obtained by simulating the loop on a digital computer were presented which show the extent to which loop nonlinearities affect the standard deviation of the frequency tracking error, the distribution of the frequency tracking error, and the loop lock range. These results show that the loop operates with a high degree of effectiveness and provide a basis for designing practical loops of the type investigated.

REFERENCES

1. Klapper, Jacob and Frankle, John T., Phase-Locked and Frequency-Feedback Systems, New York, N.Y.: Academic Press, 1972.
2. Pickard, T.B., "The Effect of Noise Upon a Method of Frequency Measurement," IRE Trans. on Information Theory, Vol. IT-4, pp. 83-88, June 1958.
3. Kobayshi, M., Osawa, H., Morinaga, N. and Namekawa, T., "On the Mean Frequency Measurement System Using Correlation Detections," IEEE Trans. on Aerospace and Electronic Systems, Vol. AES10, p. 364, May 1974.
4. Arthurs, E. and Dym, H., "On the Optimal Detection of Digital Signals in the Presence of White Gaussian Noise - A Geometrical Interpretation and a Study of Three Basic Data Transmission Systems," IRE Trans. on Communications Systems, Vol. CS-10, pp. 336-372, December 1962.
5. Miller, T.W., "Imperfect Differential Detection of a Biphase Modulated Signal - An Experimental and Analytical Study," M.Sc. Thesis, The Ohio State University, 1971.
6. Davenport, W.B. and Root, W.L., Random Signals and Noise, New York: McGraw-Hill, pp. 147-148, 1958.
7. Huff, R.J. and Reinhard, K.L., "A Delay-Lock Loop for Tracking Pulsed-Envelop Signals," IEEE Trans. Aerospace and Electronic Systems, Vol. AES-7, pp. 478-485, May 1971.

APPENDIX A

THE HYBRID FREQUENCY TRACKING LOOP

SIMULATION PROGRAM

```
C      THE FOLLOWING IS A FORTRAN LISTING OF THE PROGRAM
C      USED TO SIMULATE THE HYBRID FREQUENCY TRACKING
C      LOOP.  THE OUT PUT IS WRITTEN INTO TWO FILES.
C      CLPOUT CONTAINS THE SAMPLE MEAN OF THE LOOP
C      ERROR SIGNAL, THE STANDARD DEVIATION BASED ON THE
C      SAMPLE VARIANCE, AND POINTS ON THE
C      ASSOCIATED DISTRIBUTION FUNCTION
C      FOR A GIVEN SET OF LOOP PARAMETERS.  OUTCLP
C      PROVIDES AN INDICATION OF FALSE LOCK.
C
C
C
C
C      GAUSS IS A RANDOM NUMBER GENERATOR THAT OUTPUTS
C      INDEPENDANT SAMPLES FROM A GAUSSIAN DISTRIBUTION
C      WITH THE SPECIFIED MEAN AND STANDARD DEVIATION
C      IX IS AN ODD INTERGER USED AS A STARTING VALUE
C      S IS THE STANDARD DEVIATION
C      AMU IS THE MEAN
C      V IS THE OUTPUT VALUE
       SUBROUTINE GAUSS(IX,S,AMU,V)
       A=0.0
       DO 50 IZ=1,48
       IY=IX*16645
       IF(IY)5,6,6
     5 IY=IY+8388607+1
     6 Y=IY
       Y=Y*.1192093E-6
       IX=IY
    50 A=A+Y
       V=(A-24.0)*.5*S+AMU
       RETURN
       END
C      MAIN PROGRAM
       REAL L
       DIMENSION DELTA(6200)
       CALL ASSIGN (6HCLPOUT,6H3364S ,5)
       CALL ASSIGN (6HOUTCLP,6H3364S ,6)
       CALL DEASSN
       WRITE(5,101)
  101  FORMAT(12X,"SNR DB",14X,"MEAN",17X,"DEVIATION")
       DO 6 J=1,1
C      ESTABLISH LOOP PARAMETERS
C      X IS THE ENERGY TO NOISE DENSITY RATIO IN DB.
C      TP IS THE INTEGRATION TIME
C      G IS THE LOOP GAIN
       X=6.
       IF(X.EQ.-1.) GO TO 7
       NUN=0
       NOV=0
```

```
      EP=10.**(X/10.)
      TP=5.1370E-5
      G=1./TP*0.25
      WLO1=0.0
      PI=-ATAN2(0.,-1.)
C     THE FOLLOWING STATEMENT DETERMINES THE NUMBER
C     OF ITERATIONS FOR THE LOOP
      DO 3 K=1,6200
C     WC IS THE INPUT FREQUENCY FUNCTION
      WC=1.0E+4
      DELTA(K)=WC-WLO1
      OFST=(WC-WLO1)*TP
C     DETECT FALSE LOCK
 10   IF(OFST.LT.-PI) GO TO 8
 11   IF(OFST.GT.PI) GO TO 9
      GO TO 2
 8    NUN=NUN+1
      GO TO 2
 9    NOV=NOV+1
C     FORM SAMPLES USED FOR INPUT TO THE ESTIMATE ROUTINE
 2    L=SQRT(EP)*SIN(OFST/2.)/(OFST/2.)
      S=SQRT(.5)
 4    CALL GAUSS(4629,S,0.0,R1)
      Z1=L+R1
      CALL GAUSS(4629,S,0.0,R2)
      Z2=R2
      CALL GAUSS(4629,S,0.0,R3)
      Z3=L*COS (OFST)+R3
      CALL GAUSS(4629,S,0.0,R4)
      Z4=-L*SIN(OFST)+R4
      AG1=Z1*Z4-Z3*Z2
      AG2=Z1*Z3+Z2*Z4
C     THE FOLLOWING STATEMENT IS THE ESTIMATE FUNCTION
C     THE EQUATIONS FOR VARIOUS ESTIMATORS ARE AS FOLLOWS
C     THE LINEAR ESTIMATOR
C     WO1=ATAN2(AG1,AG2)
C     THE LINEAR ESTIMATOR WITH DECREASED LOCK RANGE
C     WO1=ATAN(AG1/AG2)
C     THE TANGENT FUNCTION ESTIMATOR
C     WO1=AG1/AG2
C     THE TANGENT FUNCTION ESTIMATOR WITH INCREASED
C     LOCK RANGE
C     WO1=AG1/ABS(AG2)
C     FOR THE ABOVE ESTIMATOR WITH LIMITS ON
C     THE OUTPUT USE SUBROUTINE CLAMP
C     THE SINE FUNCTION ESTIMATOR
C     WO1=AG1/SQRT(AG1**2+AG2**2)
      CALL CLAMP(AG1,AG2,WO1,PI)
      WO2=-WO1
      WL02=WLO1
```

```
101         WLO1=WLO2+G*WO2
102         SUM2=0.0
103    3    SUM=0.0
104    C    CALCULATE STATISTICS
105         DO 50 K=100,6200
106    50   SUM2=SUM2+DELTA(K)
107         EANN=SUM2/6100.
108         DO 5 K=100,6100
109    5    SUM=SUM+(DELTA(K)-EANN)**2
110         EAN=SUM2/6100.*TP/2/PI
111         VAR=SUM/6100.
112         DIV=SQRT(VAR)*TP/2/PI
113    100  FORMAT(3F20.6)
114         WRITE(6,-) X,NUN,NOV
115    6    WRITE(5,100) X,EAN,DIV
116         CALL STATS1 (DELTA,TP)
117    7    CALL EXIT
118         END
119    C    CLAMP IS USED AS THE ESTIMATE ROUTINE WHEN
120    C    LIMITS ARE PLACED ON THE OUTPUT OF THE TANGENT
121    C    FUNCTION ESTIMATOR WITH INCREASED LOCK RANGE
122    C    AG1 IS THE MAGNITUDE OF THE VECTOR CROSS PRODUCT
123    C    AG2 IS THE VECTOR DOT PRODUCT
124    C    WO1 IS THE OUTPUT ESTIMATE
125         SUBROUTINE CLAMP(AG1,AG2,WO1,PI)
126         ALIMIT=PI/4.
127         TSTLIM=AG1/ABS(AG2)
128         IF(TSTLIM.GT.SIN(ALIMIT)/COS(ALIMIT)) GO TO 50
129         IF(TSTLIM.LT.-SIN(ALIMIT)/COS(ALIMIT)) GO TO 51
130         WO1=TSTLIM
131         GO TO 52
132    50   WO1=SIN(ALIMIT)/COS(ALIMIT)
133         GO TO 52
134    51   WO1=-SIN(ALIMIT)/COS(ALIMIT)
135    52   RETURN
136         END
137    C    STATS1 IS USED TO CALCULATE POINTS ON THE
138    C    DISTRIBUTION FUNCTION OF THE ERROR DATA
139    C    DELTA IS THE ARRAY OF ERROR VALUES
140    C    TP IS THE INTEGRATION TIME
141         SUBROUTINE STATS1 (DELTA,TP)
142         DIMENSION DELTA(6200),BOX(20,2)
143    C    SORT DATA BY SIZE
144    4    FLG=0.
145         DO 2 INDEX1=100,6199
146         INDEX2=INDEX1+1
147         IF(DELTA(INDEX2).GE.DELTA(INDEX1)) GO TO 2
148         TEMP=DELTA(INDEX1)
149         DELTA(INDEX1)=DELTA(INDEX2)
150         DELTA(INDEX2)=TEMP
```

```
151         FLG=FLG+1.
152    2    CONTINUE
153         IF(FLG.NE.0.) GO TO 4
154    C    QUANTIZE DATA
155         DO 9 I=1,20
156    9    BOX(I,2)=0.
157         INBX=1
158         SM=-DELTA(100)
159         CH=AMAX1(SM,DELTA(6200))
160         WRITE(5,101) DELTA(100),DELTA(6200),SM,CH
161    101  FORMAT(4E13.4)
162         DO 1 INDEX3=100,6200
163    12   EDPT=-CH+INBX*.1*CH
164         BOX(INBX,1)=EDPT*TP/2./(-ATAN2(0.,-1.))
165         IF(DELTA(INDEX3).GT.EDPT) GO TO 3
166    5    BOX(INBX,2)=BOX(INBX,2)+1.
167         GO TO 1
168    3    INBX=INBX+1
169         IF(INBX.GT.20) GO TO 6
170         GO TO 12
171    1    CONTINUE
172    C    CALCULATE DISTRIBUTION POINTS
173    6    RUNTOT=0.
174         DO 7 I=1,20
175         BOX(I,2)=BOX(I,2)+RUNTOT
176    7    RUNTOT=BOX(I,2)
177         DO 8 J=1,20
178    8    BOX(J,2)=BOX(J,2)/RUNTOT*100.
179         DO 10 J2=1,20
180    10   WRITE(5,1000) BOX(J2,1),BOX(J2,2)
181    1000 FORMAT(E12.4,F10.3)
182         END$
```

APPENDIX B

CALCULATION OF THE NUMBER OF SAMPLE VALUES NEEDED FOR ACCURATE SIMULATION RESULTS

The number of sample values of radian frequency error $\Delta\omega(m)$ needed to obtain an accurate estimate of the variance of $\Delta\omega(m)$ is determined in this appendix through the use of confidence interval theory. It is assumed that $\Delta\omega(m)$ is a Gaussian random variable with a mean $\mu_{\Delta\omega}$ and variance $\sigma^2_{\Delta\omega}$. It is known that the variable defined by

$$X_k \triangleq \frac{\sum_{m=1}^{k} [\Delta\omega(m) - \overline{\Delta\omega}]^2}{\sigma^2_{\Delta\omega}} \tag{77}$$

where

$$\overline{\Delta\omega} \triangleq \frac{\sum_{m=1}^{k} \Delta\omega(m)}{k} \tag{78}$$

and k denotes the sample size is a chi square variable with k-1 degrees of freedom. If k is large, then the variable defined by

$$Y_k \triangleq \frac{X_k - k+1}{\sqrt{2(k-1)}} \tag{79}$$

is Gaussian with zero mean and unit variance. An interval with end points a and b is defined such that Y_k will be found in this interval 99% of the time:

$$(80) \qquad P_r[a < Y_k < b] \triangleq 0.99 \quad .$$

Using standard tables, the values of a and b are determined to be

$$(81) \qquad -a = b = 2.576 \quad .$$

Thus,

$$(82) \qquad P_r[-2.576 < Y_k < 2.576] = 0.99 \quad .$$

By using Eqs. (77) and (79) in the above expression an interval containing the sample variance with probability 0.99 can be expressed as

$$(83) \qquad P_r\left[\frac{k-1-2.576\sqrt{2(k-1)}}{k} \cdot \sigma^2_{\Delta\omega} < V^2 < \frac{k-1+2.576\sqrt{2(k-1)}}{k} \sigma^2_{\Delta\omega}\right] = 0.99$$

where V^2 is the sample variance given by

$$(84) \qquad V^2 = \frac{\sum_{m=1}^{k} [\Delta\omega(m) - \overline{\Delta\omega}]^2}{k} \quad .$$

The desired maximum error in this sample variance is now specified to be ±5% of the true variance. The desired interval becomes

$$(85) \qquad 0.95\ \sigma^2_{\Delta\omega} < V^2 < 1.05\ \sigma^2_{\Delta\omega}$$

Finally, the desired interval end points are equated to the confidence interval end points and the resulting equations are solved for k. Choosing the largest result gives

(86) $k = 5348$

This result is interpreted to mean that at least 5348 samples must be used so that the sample variance will not be in error by more than ±5% for 99% of the variances calculated.

MISSION
of
Rome Air Development Center

RADC plans and executes research, development, test and selected acquisition programs in support of Command, Control Communications and Intelligence (C^3I) activities. Technical and engineering support within areas of technical competence is provided to ESD Program Offices (POs) and other ESD elements. The principal technical mission areas are communications, electromagnetic guidance and control, surveillance of ground and aerospace objects, intelligence data collection and handling, information system technology, ionospheric propagation, solid state sciences, microwave physics and electronic reliability, maintainability and compatibility.